Molecular Pharmacology Fast Forward. Published on October 6, 2010 as DOI: 10.1124/mol.110.066928
This article has not been copyedited and formatted. The final version may differ from this version.
Molecular Pharmacology Fast Forward. Published on October 6, 2010 as doi:10.1124/mol.110.066928

MOL Manuscript # 66928

Development of a selective small-molecule inhibitor of Kir1.1, the Renal Outer Medullary Potassium Channel

Gautam Bhave, Brian A. Chauder, Wen Liu, Eric S. Dawson, Rishin Kadakia, Thuy, T. Nguyen, L. Michelle Lewis, Jens Meiler, C. David Weaver, Lisa M. Satlin, Craig W. Lindsley, and Jerod S. Denton

Departments of Anesthesiology (G.B., R.K., T.T.N., J.S.D.), Pharmacology (T.T.N., J.M., C.D.W., J.S.D.), Division of Nephrology (G.B.), Institute of Chemical Biology (B.A.C., E.S.D., L.M.L., C.W.L.), Digestive Disease Research Center (J.S.D.), Vanderbilt University School of Medicine, Nashville, TN, 37232; Division of Pediatric Nephrology (W.L., L.M.S.), Department of Pediatrics, Mount Sinai School of Medicine, New York, N.Y., 10029

Downloaded from molpharm.aspetjournals.org at ASPET Journals on April 18, 2024

Copyright 2010 by the American Society for Pharmacology and Experimental Therapeutics.

Molecular Pharmacology Fast Forward. Published on October 6, 2010 as DOI: 10.1124/mol.110.066928
This article has not been copyedited and formatted. The final version may differ from this version.

Running title: VU591: A Selective ROMK Channel Inhibitor

†Address correspondence to:

Jerod S. Denton, Ph.D.

T4202 Medical Center North

1161 21st Avenue South

Nashville, TN 37232

Jerod.S.Denton@Vanderbilt.Edu

PAGES:	36
TABLES:	2
SUPPLEMENTAL TABLES:	1
FIGURES:	5
SUPPLEMENTAL FIGURES:	6
REFERENCES:	31
WORDS IN ABSTRACT:	152
WORDS IN INTRODUCTION:	373
WORDS IN DISCUSSION:	1,041

NON-STANDARD ABBREVIATIONS: CD, collecting duct; CNT, connecting tubule; HTS, High throughput screening; Kir, Inward rectifying potassium; ROMK, Renal Outer Medullary K^+ Channel; TAL, thick ascending loop of Henle; TEA, tetraethylammonium; TPNQ, tertiapin-Q; 4-AP, 4-aminopyridine

Downloaded from molpharm.aspetjournals.org at ASPET Journals on April 18, 2024

Molecular Pharmacology Fast Forward. Published on October 6, 2010 as DOI: 10.1124/mol.110.066928
This article has not been copyedited and formatted. The final version may differ from this version.

ABSTRACT

The Renal Outer Medullary potassium (K^+) channel, ROMK (Kir1.1), is a putative drug target for a novel class of loop diuretic that would lower blood volume and pressure without causing hypokalemia. However, the lack of selective ROMK inhibitors has hindered efforts to assess its therapeutic potential. In a high-throughput screen for small-molecule modulators of ROMK, we previously identified a potent and moderately selective ROMK antagonist, VU590, which also inhibits Kir7.1. Because ROMK and Kir7.1 are co-expressed in the nephron, VU590 is not a good probe of ROMK function in the kidney. Here we describe the development of a structurally related inhibitor termed VU591 that is equally potent as VU590, but is selective for ROMK over Kir7.1 and more than 65 other potential off-targets. VU591 appears to block the intracellular pore of the channel. The development of VU591 may enable studies to explore the viability of ROMK as a diuretic target.

Downloaded from molpharm.aspetjournals.org at ASPET Journals on April 18, 2024

Molecular Pharmacology Fast Forward. Published on October 6, 2010 as DOI: 10.1124/mol.110.066928
This article has not been copyedited and formatted. The final version may differ from this version.

INTRODUCTION

ROMK (Kir1.1) channels are expressed in the thick ascending limb (TAL) of Henle's loop, connecting tubule (CNT) and collecting duct (CD) segments of the nephron where they mediate K^+ secretion into the urinary filtrate (reviewed in Hebert et al., 2005; Welling and Ho, 2009). In the TAL, ROMK provides substrate K^+ ions necessary for NaCl reabsorption by the Na^+-K^+-$2Cl^-$ cotransporter and loop diuretic target NKCC2. In the CNT and CD, ROMK constitutes a key pathway for K^+ secretion. A growing body of genetic (Ji et al., 2008; Tobin et al., 2008) and pharmacologic (Clark et al., 1993; Wang et al., 1995a; Wang et al., 1995b) evidence suggests that ROMK antagonists could act as potent diuretics by inhibiting Na^+ reabsorption in the TAL, while minimizing urinary K^+ loss through their actions in the CD. Thus, ROMK-directed diuretics hold the potential to avoid hypokalemia, a serious side effect of conventional loop and thiazide diuretics used in the treatment of hypertension and congestive heart failure (Grobbee and Hoes, 1995; Macdonald and Struthers, 2004).

The idea that ROMK antagonists will induce diuresis with minimal K^+ wasting is not new. In the 1990's, Giebisch and colleagues (Wang et al., 1995a; Wang et al., 1995b) as well as investigators at Upjohn Laboratories (Clark et al., 1993) characterized the renal consequences of two K_{ATP} blockers exhibiting comparatively weak off-target activity toward apical TAL and CD small conductance K^+ channels, which are now known to be mediated at least in part by ROMK. At high doses, these compounds induced natriuresis and diuresis, but had very little effect on urinary K^+ excretion. While these studies provided a glimpse into the therapeutic potential of ROMK, the agents were limited by low potency toward ROMK and undesirable cardiovascular and metabolic side effects mediated by K_{ATP} channels.

Downloaded from molpharm.aspetjournals.org at ASPET Journals on April 18, 2024

Molecular Pharmacology Fast Forward. Published on October 6, 2010 as DOI: 10.1124/mol.110.066928
This article has not been copyedited and formatted. The final version may differ from this version.

We recently performed a high-throughput screen (HTS) of approximately 125,000 small molecules for chemical modulators of ROMK (Lewis et al., 2009). Several antagonists were discovered, including a sub-micromolar ROMK inhibitor termed VU590 that also weakly inhibits Kir7.1. Because ROMK and Kir7.1 are co-expressed in the nephron, VU590 cannot be used as a selective ROMK probe in the kidney. Here we describe the development of a novel inhibitor termed VU591 that is equally potent and highly selective for ROMK.

Downloaded from molpharm.aspetjournals.org at ASPET Journals on April 18, 2024

Molecular Pharmacology Fast Forward. Published on October 6, 2010 as DOI: 10.1124/mol.110.066928
This article has not been copyedited and formatted. The final version may differ from this version.

MATERIALS AND METHODS

Expression Vectors. Plasmids used in this study are from the following sources: rat ROMK1 (NM_017023; Chun Jiang, Georgia State University), human Kir2.1 (NM_000891.2; Al George, Vanderbilt University School of Medicine), human Kir7.1 (NM_002242.2; David Clapham, Harvard Medical School), human Slo1/KCNMA1 (NM_001014797; Jianmin Cui, Washington University), human KCNMB1 (NM_004137; Robert Brenner, University of Texas Health Science Center at San Antonio), human eag-related gene (hERG; Sabina Kupershmidt, Vanderbilt); mouse Kir6.2 (NM_010602) and hamster SUR1 (L40623.1) vectors are from Colin Nichols (Washington University). Human ROMK1 (NM_000220), Kir2.3 (NM_152868), Kir4.1 (NM_002241) and Kv1.3 (NM_002232.2) were purchased from OriGene Technologies (Rockville, MD).

Cell Lines and Transfections. Thallium **(**Tl^+)-flux assays and parallel patch clamp experiments (see below) were performed using the C1 monoclonal tetracycline-regulateable HEK-293 cell line expressing ROMK1-S44D described previously (Lewis et al., 2009). For conventional patch clamp experiments, HEK-293 cells (CRL-1573; ATCC; Manassas, VA) were transiently co-transfected with channel expression vector and pcDNA3.1-EGFP (transfection marker) using Lipofectamine 2000 (Invitrogen, Carlsbad, CA) as described previously (Fallen et al., 2009) or FuGENE 6 (Roche Applied Science, Indianapolis, IN) according to the manufacturer's instructions.

Thallium Flux Assays. Tl^+ flux assays were performed as described in detail previously (Lewis et al., 2009). Briefly, C1 cells cultured overnight in a 384-well plate containing

Downloaded from molpharm.aspetjournals.org at ASPET Journals on April 18, 2024

Molecular Pharmacology Fast Forward. Published on October 6, 2010 as DOI: 10.1124/mol.110.066928
This article has not been copyedited and formatted. The final version may differ from this version.

serum-free media and tetracycline were loaded with the Tl^+-sensitive fluorescent dye FluxOR (Invitrogen). Assays were performed on a Hamamatsu Functional Drug Screening System 6000. Cells were incubated for 20 min with small-molecules prior to Tl^+ addition. The normalized rate of flux between 7 and 12 seconds following Tl^+ addition is reported.

Conventional Patch Clamp Electrophysiology. Conventional patch clamp experiments were performed essentially as described previously (Fallen et al., 2009). The standard intracellular solution contained (in mM): 135 KCl, 2 $MgCl_2$, 1 EGTA, 10 HEPES-K, 2 Na_2ATP (Roche), pH 7.3, adjust to 275 mOsm with sucrose. For Kir2.3 recordings, $MgCl_2$ was reduced to 1 mM to prevent channel rundown (Chuang et al., 1997). Kir6.2 recordings were made with 0.5 mM $MgCl_2$ in the absence of ATP to eliminate ATP induced channel inhibition. Slo1/β1 recordings were conducted with 1 mM EGTA and 0.1 mM $CaCl_2$ without ATP or $MgCl_2$. The standard bath solution contained (in mM): 135 NaCl, 5 KCl, 2 $CaCl_2$, 1 $MgCl_2$, 5 glucose, 10 HEPES-Na, pH 7.4, 290 mOsm. In some experiments, a high-K^+ bath containing the following (in mM) was used: 90 NaCl, 50 KCl, 2 $CaCl_2$, 1 $MgCl_2$, 5 glucose, 10 HEPES-Na, pH 7.4, 290 mOsm.

For Kir current recordings, cells were voltage clamped and stepped every 5 sec from a holding potential of -75 mV to -120 mV for 200 msec, then ramped at a rate of 2.4 mV/msec to 120 mV before returning to -75 mV (Fig. 2C inset). Kv1.3 currents were evoked using a similar protocol, except Vm was ramped from -120 mV to 0 mV every 10 sec. Slo1/β1 currents were recorded every 5 sec after 200 ms voltage step to 100 mV from a holding potential of -75 mV.

Downloaded from molpharm.aspetjournals.org at ASPET Journals on April 18, 2024

Molecular Pharmacology Fast Forward. Published on October 6, 2010 as DOI: 10.1124/mol.110.066928
This article has not been copyedited and formatted. The final version may differ from this version.

After achieving stable whole-cell currents, VU591 was applied intermittently or continuously for 4-10 min. This was followed by application of a known channel blocker (i.e. 2 mM barium, Kir channels; 2 mM tetraethylammonium [TEA], Slo1/β1 channels;1 mM 4-aminopyridine [4-AP], Kv1.3; or Dofetilide, hERG) as a positive control.

Automated Patch Clamp Electrophysiology. Parallel patch clamp experiments were performed using a Patchliner workstation (Nanion Technologies; Munich, Germany) which enables fully automated patch clamp recordings to be made from up to 8 cells simultaneously (Milligan et al., 2009). The Patchliner utilizes disposable NPC-16© microfluidic recording chambers containing an array of 16 individual planar glass electrodes with apertures of defined geometry and resistance. Medium-resistance (1.8-3.0 MΩ) chambers were used in the present study. Eight channels can be recorded from concurrently using 2 HEKA EPC-10 Quadro amplifiers. A programmable robotic probe is used for solution exchanges. A typical experiment was performed as follows. The lower (35 µl volume) and upper (15 µl volume) chambers were filled with intracellular and extracellular recording solutions, respectively. The intracellular solution contained (in mM): 50 KCl, 10 NaCl, 60 KFl, 2 $MgCl_2$, 10 EGTA, 20 HEPES, pH 7.2, 275 mOsm). The standard extracellular solution was identical to that used for conventional patch clamp experiments described above. Overnight tetracycline-induced C1 cells (Lewis et al., 2009) were dissociated by brief trypsinization, diluted to a concentration of 10^6 cells/ml and added to the upper chamber of the recording chamber where one cell is pulled by gentle suction into the aperture separating the two compartments. A series of automated vacuum steps is delivered to the internal chamber to establish a giga-ohm seal and whole-cell access. A "seal enhancer" solution containing (in mM): 80 NaCl, 3 KCl,

Downloaded from molpharm.aspetjournals.org at ASPET Journals on April 18, 2024

Molecular Pharmacology Fast Forward. Published on October 6, 2010 as DOI: 10.1124/mol.110.066928
This article has not been copyedited and formatted. The final version may differ from this version.

10 $MgCl_2$, 35 $CaCl_2$, 10 HEPES (pH 7.4) is added to the external compartment to facilitate seal formation. After establishing the whole-cell configuration, seal enhancer was exchanged for standard bath solution and the voltage clamp experiment was initiated. Cells were voltage clamped from a -75 mM holding potential and stepped for 200 msec every 10 sec to a test pulse of -120 mV. For dose-response experiments, 45 µl of test compounds of increasing concentration were added to the external compartment followed by a final addition of 2 mM Ba^{2+} to measure leak current. Cells exhibiting an unstable baseline or less than 90% Ba^{2+}-inhibitable current at -120 mV were excluded from analysis.

Preparation of *Xenopus laevis* oocytes. Stage V-VI oocytes from the African clawed frog *Xenopus laevis* were generously provided by Dr. Eric Delpire (Vanderbilt University School of Medicine). The oocyte follicle layer was removed by manual dissection following enzymatic treatment with 2 mg/ml collagenase (Type 1A Sigma) dissolved in calcium-free OR-2 of the following composition (in mM): 82.5 NaCl, 2 KCl, 1 $MgCl_2$, 5 HEPES, with pH 7.5 adjusted with NaOH. Oocytes were allowed to recover overnight at 16°C in L-15 media diluted 50% with 18 MΩ water and containing gentamicin sulfate (25 mg/ml).

RNA transcription and injection. A plasmid encoding the human *eag*-related gene (hERG) was linearized with EcoRI and used as a template to transcribe 7-methyl guanosine-capped RNA (cRNA) with the SP6 RNA polymerase and nucleotides provided in the mMESSAGE mMACHINE kit (Ambion, Austin, TX). cRNA was purified by LiCl precipitation, diluted in RNAase-free water and used for injections. Five to fifty ng of

Downloaded from molpharm.aspetjournals.org at ASPET Journals on April 18, 2024

Molecular Pharmacology Fast Forward. Published on October 6, 2010 as DOI: 10.1124/mol.110.066928
This article has not been copyedited and formatted. The final version may differ from this version.

hERG cRNA in 50 nl of water was injected into each oocyte using a Drummond digital microdispenser. Oocytes were incubated at 16˚C in modified L-15 for 24-48 h prior to hERG recordings.

Two-electrode voltage-clamp analysis. Whole-cell currents were recorded from *Xenopus* oocytes injected with hERG cRNA using the two-electrode voltage clamp technique. Current and voltage commands were generated with a GeneClamp 600 amplifier, a Digidata 1200 A/D converter and pClamp 8.0 software (Molecular Devices, Sunnyvale, CA). The bath was actively clamped to 0 mV using a VG-2A bath clamp (Molecular Devices). Electrodes pulled from borosilicate glass (Sutter Instruments, Novato, CA) using a PP-830 vertical puller (Narishige International, Narishige, Japan) had resistances of 0.5-5.0 MΩ when filled with 3 M KCl. The standard bath solution contained (in mM): 85 NaCl, 5 KCl, 10 HEPES, 2 $MgCl_2$, pH 7.4 with NaOH. VU591 and the hERG channel inhibitor Dofetilide (positive control; Tocris Biosciencces) were tested at 10 μM.

hERG currents were evoked as follows. From a holding potential of -80 mV, the oocyte potential was stepped to -20 mV for 2 sec and returned to -80 mV to elicit inward hERG tail currents. This protocol was repeated every 20-30 sec. hERG currents were pharmacologically isolated from endogenous oocytes currents by subtracting the tail current at -80 mV from the time-independent current remaining after maximal hERG blockade with 10 μM Dofetilide (Supplemental Figure 5).

Chemical Synthesis.

1,3-bis(5-nitro-1H-benzo[d]imidazol-2-yl)propane (BNBI):

Downloaded from molpharm.aspetjournals.org at ASPET Journals on April 18, 2024

Molecular Pharmacology Fast Forward. Published on October 6, 2010 as DOI: 10.1124/mol.110.066928
This article has not been copyedited and formatted. The final version may differ from this version.

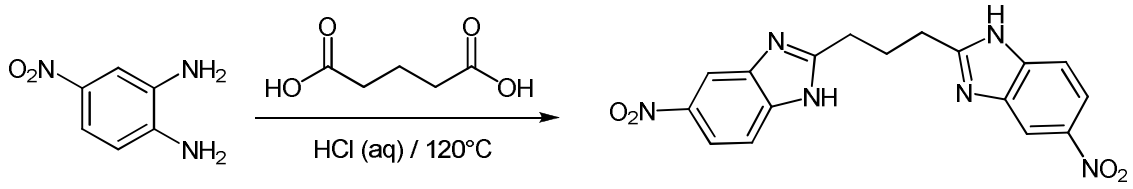

A suspension of 4-nitrobenzene-1,2-diamine (300 mg, 1.96 mmol) and glutaric acid (130 mg, 0.98 mmol) in 5N HCl (2 mL) was heated to 120°C (bath temp) in a sealed tube. A solution forms in 1 h. After 12 h of heating, the mixture was cooled to rt and poured into saturated $NaHCO_3$ solution (50 mL) and the pH was adjusted to 8. The mixture was filtered and the product was washed with water. The product was dried in a vacuum oven for 10 h to afford BNBI as a light brown solid (260 mg, 72%). The product was recrystallized from absolute EtOH to give BNBI as a colorless solid. ^{1}H-NMR (400 MHz, DMSO-d_6) δ 8.37(d, *J*=2.1 Hz, 2H), 8.11 (dd, *J*=8.8, 2.1 Hz, 2H), 7.69 (d, *J*=8.8 Hz, 2H), 3.10 (t, J=7.3 Hz, 4H), 2.42 (q, J=7.3 Hz, 2H); LCMS (m/z) = 367 (M+H).

2,2'-oxybis(methylene)bis(5-nitro-1H-benzo[d]imidazole) (VU591):

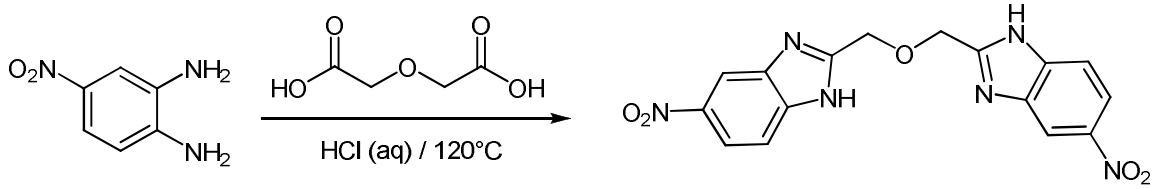

A suspension of 4-nitrobenzene-1,2-diamine (300 mg, 1.96 mmol) and diglycolic acid (131 mg, 0.98 mmol) in 5N HCl (2 mL) was heated to 120°C (bath temp) in a sealed tube. A solution forms in 1 h. After 12 h of heating, the mixture was cooled to rt and poured into sat. $NaHCO_3$ solution (50 mL) and the pH was adjusted to 8. The mixture was filtered and the product was washed with water. The product was dried in a vacuum

Downloaded from molpharm.aspetjournals.org at ASPET Journals on April 18, 2024

Molecular Pharmacology Fast Forward. Published on October 6, 2010 as DOI: 10.1124/mol.110.066928
This article has not been copyedited and formatted. The final version may differ from this version.

oven for 10 h to afford VU591 as a light brown solid (368 mg, 51%). The product was recrystallized from absolute EtOH to give VU591 as a colorless solid. ^{1}H-NMR (400 MHz, DMSO-d_6) δ 8.46 (d, *J*=1.3 Hz, 2H), 8.11 (dd, *J*=8.8, 1.3 Hz, 2H), 7.73 (d, *J*=8.8 Hz, 2H), 5.00 (s, 4H); HRMS (calculated for $C_{16}H_{12}N_6O_5$+H) 369.0947; Found 369.0947.

7,13-bis(4-nitrobenzyl)-1,4,10-trioxa-7,13-diazacyclopentadecane (VU590):

VU590 used in this study was synthesized locally as described previously (Lewis *et al.*, 2009). However, VU590 is now commercially available from Sigma-Aldrich (cat. number V4265) and Tocris Bioscience (cat. number 3891).

Plasma protein binding: Human or rat plasma samples spiked with 10 mM of VU591, Warfarin (control) or Verapamil (control) dissolved in DMSO were added in the cis chambers of Rapid Equilibrium Dialysis plates (Thermo Fisher,USA). Dulbecco's phosphate buffered saline was added to the corresponding trans compartment. The samples were dialyzed for 4h at 37°C with shaking, after which the proteins were extracted using ice cold acetonitrile containing 0.1% formic acid and an internal standard at a concentration of 50 ng/ml. The extracts were analyzed by means of HPLC/MS/MS, using a ThermoFinnigan TSQ Quantum Ultra (Thermo Fisher Scientific, Waltham, MA) mass spectrometer operating in the positive ion mode, by selective reaction monitoring. Percent unbound VU591 was calculated based on the percentage of compound in the PBS chamber compared to that of the total in the PBS and plasma chambers.

Downloaded from molpharm.aspetjournals.org at ASPET Journals on April 18, 2024

Molecular Pharmacology Fast Forward. Published on October 6, 2010 as DOI: 10.1124/mol.110.066928
This article has not been copyedited and formatted. The final version may differ from this version.

Metabolic stability. VU591, Verapamil (control) or Propranalol (control) were incubated at 37˚C for 15 min with constant shaking in solution containing rat or human liver microsomes, phosphate buffered saline and NADPH as a cofactor. Following incubation, the samples were extracted using ice-cold acetonitrile containing 0.1% formic acid and an internal standard. The extracts were analyzed by means of HPLC/MS/MS. Percent test compound remaining following incubation was calculated based on the amount of compound in the incubated samples compared to identically prepared control samples not incubated with microsomes.

Molecular Modeling. SurflexSim (SybylX 1.1; Tripos International, 1699 South Hanley Rd., St. Louis, Missouri, 63144, USA) was applied to generate 100 mutual flexible alignment hypotheses for the three-dimensional superposition of BNBI and VU591. The algorithm is based on morphological similarity, a method that attempts to gauge molecular similarity from the point of view of the protein target via a fragment-based flexible alignment of small molecules with known activity. Briefly, this method makes use of a three-dimensional grid of observer points in which minimum distances to the van der Waals surface, a hydrogen-bond acceptor or negatively charged atom, and a hydrogen-bond donor or positively charged atom are employed in conformational sampling with the addition of a restraining term to prevent excessive steric clash and a directionality term to capture observations of polar features (Jain, 2000). The best scoring alignment for BNBI/VU591 was taken as a template for the flexible alignment of VU590 using SurflexSim to explore the potential three-dimensional conformational similarity of these molecules. Visualization of surface electrostatic properties for VU590, BNBI and VU591 was performed by mapping atom-centered partial charges

Downloaded from molpharm.aspetjournals.org at ASPET Journals on April 18, 2024

Molecular Pharmacology Fast Forward. Published on October 6, 2010 as DOI: 10.1124/mol.110.066928
This article has not been copyedited and formatted. The final version may differ from this version.

from the Merck Molecular Mechanics Force Field (MMFF94) onto Connolly surfaces that were generated for the most similar conformers of each compound and rendered in PyMol (DeLano, W.L. The PyMOL Molecular Graphics System. (2008) DeLano Scientific LLC, Palo Alto, CA, USA. http://www.pymol.org).

Statistics. Unless noted otherwise, results are expressed as means ± S.E.M.; n equals the number of replicates. To calculate the half-inhibition concentration of VU591 for rat ROMK (Table 1), the unaveraged concentration-response data from between four and seven cells at each concentration were fit to a four parameter logistic equation in Excel 2007 (Microsoft) using the XLfit add-in (ID Business Solutions). The top and bottom parameters were constrained at 100% as defined by control traces run prior to test compound exposure for each cell and 0% as defined by currents measured in four cells with a fully-effective concentration of barium. The voltage-dependence of VU591 block was assessed using univariate statistics with paired t-test conducted using commercially available statistical software (SigmaStat; SPSS Inc. Chicago, IL). Multivariate statistics used a generalized linear model (GLM) accounting for repeated measures and were performed with R-software version 2.10.0 (www.r-project.org). In all analyses, a 2-sided P-value <0.05 was required to reject the null hypothesis.

Downloaded from molpharm.aspetjournals.org at ASPET Journals on April 18, 2024

Molecular Pharmacology Fast Forward. Published on October 6, 2010 as DOI: 10.1124/mol.110.066928
This article has not been copyedited and formatted. The final version may differ from this version.

RESULTS

1,3-bis(5-nitro-1H-benzo[d]imidazol-2-yl)propane inhibits ROMK but not Kir7.1. VU590 is a bis-nitro-benzyl compound (Fig. 2A, top) that inhibits ROMK at sub-micromolar concentrations, but has no effect on Kir2.1 or Kir4.1. VU590 is only moderately selective, however, since it also inhibits Kir7.1 at low micromolar concentrations (Lewis et al., 2009). Because ROMK and Kir7.1 are co-expressed in the nephron (Ookata et al., 2000), VU590 can not be used to selectively assess ROMK function in the kidney.

In an effort to identify a more selective inhibitor, we tested a structurally related hit from the primary screen, bis-nitro benzimidazole (BNBI; Fig. 2A, middle), for activity toward ROMK and Kir7.1. BNBI was resynthesized and examined in whole-cell patch clamp experiments. Its effects on ROMK were tested in stably transfected C1 cells (see Methods) using a Patchliner parallel patch clamp workstation (Milligan et al., 2009). As shown in Fig. 1A, BNBI inhibited ROMK current at -120 mV in a dose-dependent manner at 1, 5 and 10 μM. The mean ± S.E.M concentration-response curves (CRC) for BNBI, and VU590 for comparison, are shown in Fig. 1B. Compared to VU590, ROMK inhibition by BNBI was weak and incomplete. However, we found that unlike VU590, which inhibited Kir7.1 by 58.3 ± 2.4 % (n=3) at 10 μM, BNBI at concentrations up to 100 μM had no significant ($P>0.05$; n=3) effect on Kir7.1 activity (Fig. 1C). We therefore initiated medicinal chemistry efforts around the BNBI scaffold with the goal of improving its potency while maintaining its selectivity.

Figure 2A shows the chemical structures of VU590 (top) and BNBI (middle) with sub-structural regions of similar topology highlighted in bold. Each compound contains two nitro (NO_2) groups flanking a variable 7-atom linker region harboring two nitrogen

Downloaded from molpharm.aspetjournals.org at ASPET Journals on April 18, 2024

Molecular Pharmacology Fast Forward. Published on October 6, 2010 as DOI: 10.1124/mol.110.066928
This article has not been copyedited and formatted. The final version may differ from this version.

atoms. A key difference between VU590 and BNBI is the absence of a central oxygen atom within the linker of BNBI. Given the increased polarity and hydrogen bond acceptor potential of the VU590 linker, we hypothesized that the addition of an ether oxygen to the BNBI linker would increase potency toward ROMK by providing additional interactions between the channel and ether oxygen lone pair electrons (see Discussion). Indeed, the resulting compound, 2,2'-oxybis(methylene)bis(5-nitro-1H-benzo[d]imidazole) (VU591; Fig. 2A, bottom), was almost 30-fold more potent at inhibiting ROMK than was BNBI. In Tl^+ flux assays, VU591 inhibited ROMK with an IC_{50} of 240 nM, whereas BNBI inhibited ROMK with a IC_{50} of approximately 8 μM (Fig. 2B).

VU591 is a selective ROMK inhibitor. We next examined the selectivity of VU591 across several inward rectifier and voltage-gated K^+ channels expressed in HEK-293 cells. Cells were voltage ramped between -120 mV and 120 mV every 5 sec from holding potential of -75 mV (Fig. 2C, inset). ROMK-mediated inward current at -120 mV was inhibited by 10 μM VU591 with a monoexponential time course. Washout was very slow and incomplete, and the presence of VU591 did not prevent additional block by extracellular barium (Fig. 2C). As illustrated in Fig. 2D, and quantified in Fig. 3C, VU591 block in a physiological K^+ gradient (5 mM extracellular 135 mM intracellular) was effective at both negative and positive potentials.

Consistent with the Tl^+ flux data (Fig. 2B), VU591 inhibited rat ROMK dose-dependently with an IC_{50} of 300 nM (Table 1), which is virtually identical to that of VU590 (IC_{50} 290 nM; Lewis et al., 2009). Thus, VU591 does not significantly improve upon VU590's potency toward ROMK. Block by VU591 reached a maximum of

Downloaded from molpharm.aspetjournals.org at ASPET Journals on April 18, 2024

Molecular Pharmacology Fast Forward. Published on October 6, 2010 as DOI: 10.1124/mol.110.066928
This article has not been copyedited and formatted. The final version may differ from this version.

approximately 90% at 10 μM, as block by 30 μM VU591 was not significantly (P>0.05) different (Table 1). VU591 also blocked human ROMK. VU591 had no effect on Kir7.1 at 10 μM, a concentration at which VU590 inhibited the channel by ~60% (Fig. 1C), nor did it inhibit Kir2.1, Kir2.3 and Kir4.1. At 10 μM and 50 μM, respectively, VU591 inhibited Kir6.2/SUR1 currents by 17 ± 4 % and 28 ± 3 % (Table 1), which still affords a 150-fold selectivity window for ROMK over Kir6.2/SUR1. Representative steady-state current traces and time course data and are shown in Supplemental Figs. 1 and 2, respectively.

We broadened our selectivity analysis to include two voltage-gated K^+ (Kv) channels that are known to contribute to K^+ secretion in the nephron: Calcium- and voltage-activated large conductance K^+ (BK) channels and Kv1.3. BK channels comprised of channel forming Slo1 (*KCNMA1*) α- and regulatory β-subunits (*KCNMB*) have emerged recently as important regulators of distal nephron K^+ secretion. Knockout studies in mice have shown that loss of Slo1 or β1 expression reduces the kaliuretic response to high urinary flow rates (Grimm and Sansom, 2007; Pluznick et al., 2003; Rieg et al., 2007). Off-target activity toward BK channels could therefore erroneously assign a role for ROMK in the physiological response to VU591. We therefore tested whether VU591 inhibits heterologously expressed Slo1/β1 BK channels. At a concentration of 10 μM, VU591 had no significant (P>0.05; n=5) effect on Slo1/β1 currents (Table 1). Representative BK current traces and a time course experiment are shown in Supplemental Fig. 3.

Kv1.3 was shown recently to contribute to K^+ secretion in the CD of rats fed a high-K diet (Carrisoza-Gaytan et al.). We therefore determined if VU591 inhibits human

Downloaded from molpharm.aspetjournals.org at ASPET Journals on April 18, 2024

Molecular Pharmacology Fast Forward. Published on October 6, 2010 as DOI: 10.1124/mol.110.066928
This article has not been copyedited and formatted. The final version may differ from this version.

Kv1.3 heterologously expressed in HEK-293 cells. As shown in Table 1, 10 μM VU591 did not inhibit Kv1.3. Representative Kv1.3 current traces and a time course experiment are shown in Supplemental Fig. 4. We previously reported (Lewis et al., 2009) that VU590 inhibits the mixed Kv current endogenously expressed in HEK-293 cells (Jiang et al., 2002; Yu and Kerchner, 1998). Messenger RNA for Kv1.3 is prominently expressed in HEK-293 cells and therefore likely contributes to the endogenous current (Jiang et al., 2002). Consistent with the Kv1.3 heterologous expression data, VU591 had no significant ($P>0.05$; n=4) effect on the native HEK-293 current (mean ± SEM current at 60 mV in control and VU591-containing buffer were 251 ± 82 pA and 256 ± 84 pA, respectively).

Analysis of potential off-target activity was expanded further to include a panel of 68 critical targets including several cardiac and CNS ion channels and receptors using the LeadProfilingScreen® system from Ricerca Biosciences (Concord, OH). In this system, radioligand displacement assays are used to screen for small molecule activity against a target of interest and values indicating percent ligand displacement are reported. VU591 had no effect on ^{3}H-astemizole binding of hERG channels, an off-target associated with lethal ventricular arrhythmias (Supplemental Table 1). However, we found in two-electrode voltage-clamp experiments on *Xenopus* oocytes, that 10 μM VU591 inhibited hERG tail currents at -80 mV (Supplemental Fig. 5) by approximately 25% (Table 1). Whether the discrepancies between radioligand binding and electrophysiological data reflect voltage- or use-dependent hERG channel block will be assessed in future studies.

Only four targets ($GABA_A$ receptor, dopamine D4 receptor, dopamine transporter, and norepinephrine transporter) exhibited greater than 50% radioligand displacement with 10 μM VU591 (Supplemental Table 1), a threshold commonly used to prioritize hits

Downloaded from molpharm.aspetjournals.org at ASPET Journals on April 18, 2024

Molecular Pharmacology Fast Forward. Published on October 6, 2010 as DOI: 10.1124/mol.110.066928
This article has not been copyedited and formatted. The final version may differ from this version.

from a HTS. These activities were further characterized with full CRCs in functional assays. Only the $GABA_A$ receptor exhibited an IC_{50} below 10 μM (IC_{50} = 6.2 μM), which still affords a 25-fold selectivity window for ROMK.

VU591 is a Pore Blocker. Given the structural similarities between VU590 and VU591 (Fig. 2A), we hypothesize they share a common binding site in ROMK. VU590 can be displaced from its binding site by inwardly directed K^+ ions, a phenomenon termed "knock-off", suggesting it blocks the intracellular pore of the channel (Lewis et al., 2009). If VU590 and VU591 interact with the same sites, we postulated that VU591 would also exhibit knock-off. To test this hypothesis, HEK-293 cells were bathed in solutions containing 5 mM or 50 mM K^+ and 10 μM VU591 to block ROMK (Fig. 3A-B). The cells were subsequently voltage clamped at a holding potential of -80 mV (5 K^+) or -20 mV (50 K^+) and then stepped for 5 seconds to test voltages between 20 and -120 mV in 20 mV increments (Fig. 3D). The mean ± SEM percent block at the end of each test pulse is shown in Fig. 3C. In 5 mM K^+, VU591 inhibition exhibited a trend towards reduced block with hyperpolarization, but was not statistically significant ($P = 0.081$). However, elevation of extracellular K^+ caused a dramatic decrease in percent block at hyperpolarizing potentials ($P<0.001$). To confirm that the hyperpolarization- and high K^+-induced current is not carried by endogenous inward rectifiers that are insensitive to VU591, we showed the current could be inhibited by the ROMK blocker tertiapin-Q (TPNQ; Fig. 3A-B, right panels). Taken together, these data support the hypothesis that the VU591 binding site lies within the intracellular ion permeation pathway near the VU590 binding site.

Downloaded from molpharm.aspetjournals.org at ASPET Journals on April 18, 2024

Molecular Pharmacology Fast Forward. Published on October 6, 2010 as DOI: 10.1124/mol.110.066928
This article has not been copyedited and formatted. The final version may differ from this version.

VU591 Serum Protein Binding and Metabolic Stability. The utility of VU591 as a probe of ROMK function in whole-animal studies will depend in part on its propensity to bind serum protein and susceptibility to degradation by liver metabolic enzymes. We therefore measured the protein binding and metabolic stability of VU591 in vitro. Binding of VU591 to human and rat serum protein was compared to the anticoagulant Warfarin, a highly protein-bound drug, and Verapamil as controls. The results, which are summarized in Table 2, show that VU591 is almost entirely protein bound in human serum, but that approximately 2% of the inhibitor is free in rat serum.

The metabolic stability of VU591, Verapamil and Propranalol in human and rat liver microsomes was assessed next. The results are summarized in Fig. 4. After a 15-min incubation period, approximately 60-80% of VU591 remained intact in rat and human microsomes. In both species, VU591 was more stable than Verapamil and Propranalol.

Downloaded from molpharm.aspetjournals.org at ASPET Journals on April 18, 2024

Molecular Pharmacology Fast Forward. Published on October 6, 2010 as DOI: 10.1124/mol.110.066928
This article has not been copyedited and formatted. The final version may differ from this version.

DISCUSSION

Since Hebert (Ho et al., 1993), Palmer (Zhou et al., 1994) and colleagues cloned ROMK nearly 20 years ago, the small-molecule pharmacology of the Kir family has remained largely undeveloped and limited to barium, cesium and a handful of non-selective drugs exhibiting weak off-target activity toward Kir channels (reviewed in (Bhave, 2010). The slow progress in the field has hindered efforts to understand the physiology, clinical relevance and therapeutic potential certain Kir channels. Part of our motivation for developing small-molecule inhibitors of ROMK is to test the long-standing hypothesis that ROMK is a target for a novel class of antihypertensive drug.

The discovery (Simon et al., 1996) of antenatal Bartter syndrome (ABS) patients carrying autosomal recessive loss-of-function mutations in the gene encoding ROMK (*KCNJ1*) seems to argue against ROMK as a viable therapeutic target. ABS patients frequently present with hypercalciuria, metabolic alkalosis and hypokalemia, in addition to low-to-normal blood pressure (Bartter et al., 1962; Peters et al., 2002). Interestingly, however, Lifton and colleagues recently identified heterozygous carriers of *KCNJ1* mutations with lower blood pressure, but no reported symptoms of ABS (Ji et al., 2008). Similarly, Tobin *et al.* (2008) identified small nucleotide polymorphisms in *KCNJ1* that were associated with lower blood pressure in the general population. No associations with serum K^+ were found (Tobin et al., 2008). Taken together, these studies suggest that a partial reduction in ROMK function may lower blood pressure without causing derangements in serum electrolytes.

It remains to be seen whether pharmacological inhibition of ROMK in genetically normal individuals will induce diuresis. The canonical 30-picoSiemen (pS) channel attributed to ROMK is co-expressed with a molecularly unidentified 70-pS channel in the

Downloaded from molpharm.aspetjournals.org at ASPET Journals on April 18, 2024

Molecular Pharmacology Fast Forward. Published on October 6, 2010 as DOI: 10.1124/mol.110.066928
This article has not been copyedited and formatted. The final version may differ from this version.

TAL, where it is estimated to contribute up to 80% of apical K^+ conductance (Wang and Lu, 1995). Like the 30-pS channel, the 70 pS channel is absent in *KCNJ1*$^{-/-}$ knockout mice, leading Lu *et al.* (2004) to propose that ROMK subunits form part of the 70-pS channel (Lu et al., 2004). Conceivably, the volume disturbances caused by mutations in *KCNJ1* reflect loss of both conductances. It will be important to determine if VU591 inhibits one or both conductances to facilitate the interpretation animal studies assessing VU591's diuretic properties. Given the selectivity of VU591 for ROMK over other inward rectifiers, we postulate that VU591 will not inhibit the 70-pS conductance if it is carried by a heteromeric channel. Testing this hypothesis should ultimately shed light on the molecular structure and physiology of the 70-pS channel.

As a first step toward determining if VU591 is active on native ROMK channels expressed in the distal nephron, we measured net K^+ (J_K) and Na^+ (J_{Na}) transport in isolated-perfused rat collecting ducts (CD) before and after luminal perfusion with 10 μM VU591. Data summarized in Supplemental Fig. 6 show that VU591 significantly inhibited J_K from -7.0 ± 1.3 (control) to -3.6 ± 0.6 (VU591) pmol/min per mm (n = 4; $P<0.05$) in CD perfused at 1.5 ± 0.4 and 1.2 ± 0.1 ($P>0.05$) nl/min per mm, respectively. Luminal VU591 had no significant effect on J_{Na} in these same tubules (16.1 ± 2.6 and 12.5 ± 0.6 pmol/min per mm; $P>0.05$). These preliminary data suggest strongly that VU591 inhibits native ROMK in rat kidney, and that ROMK mediates at least in part basal K^+ secretion in the collecting duct. VU591 used in combination with other blockers should help to elucidate the relative contribution of ROMK and other K^+ channels (e.g. BK, Kv1.3) to renal K^+ transport during various physiological and pathophysiological states.

Downloaded from molpharm.aspetjournals.org at ASPET Journals on April 18, 2024

Molecular Pharmacology Fast Forward. Published on October 6, 2010 as DOI: 10.1124/mol.110.066928
This article has not been copyedited and formatted. The final version may differ from this version.

VU591 inhibited hERG activity by approximately 25% (Table 1). Our data may actually underestimate the degree of hERG block observed in mammals because many drugs exhibit decreased potencies toward hERG expressed in *Xenopus* oocytes (Witchel et al., 2002). If VU591 is indeed a potent hERG blocker in cardiac myocytes, this may limit the choice of animal models for in vivo studies to mice, in which hERG does not play a critical role in cardiac function (Wang et al., 1996).

We found that 10-30 μM VU591 inhibited ROMK current at -120 mV by approximately 90%, raising the possibility that VU591 is a partial antagonist of the channel. However, it should be noted VU591 inhibition increased to ~97% at -60 mV (Fig. 3C). We therefore propose that VU591 is a full antagonist exhibiting weak voltage-dependent unblock at strong negative potentials. This property should have minimal effects on its potency in cells with typical resting potentials above E_K.

Why does the addition of the ether oxygen to the aliphatic linker region of BNBI (Fig. 5B) increase its potency toward ROMK? We explored this question using the SurflexSim optimized flexible alignment algorithm (see Methods), which superimposes common chemical features of VU590, BNBI and VU591, including hydrogen bond donors, electron-rich imidazole nitrogens, ether oxygens and nitrophenyl groups. The resulting structural alignments contained conformers that concentrate negative electrostatic potential by bringing together the ether oxygen and both electron-rich imidazole nitrogen atoms of VU591 (Fig. 5C) in close spatial proximity with the macrocycle ring nitrogens and an ether oxygen of VU590 (Fig. 5A). This supports the notion that the greater potency of VU591 is due to an increased electron donor potential

Downloaded from molpharm.aspetjournals.org at ASPET Journals on April 18, 2024

Molecular Pharmacology Fast Forward. Published on October 6, 2010 as DOI: 10.1124/mol.110.066928
This article has not been copyedited and formatted. The final version may differ from this version.

(and hydrogen bond acceptor potential) of the ether linker that stabilizes ligand interactions with a polar portion of the ROMK pore.

The flexible and bulky VU590 macrocycle linker (Fig. 5D) could contribute to the compound's low-affinity block of Kir7.1 (Fig. 1C). Its absence in BNBI (Fig. 5E) and VU591 (Fig. 5F) may therefore contribute toward selectivity for ROMK. The SurflexSim alignment method also minimizes non-overlapping compound volume while aligning chemical features as part of the conformational search process (see Methods). The number of VU590 conformational ensemble atoms lying outside of the Connolly surface of the optimized BNBI/VU591 alignment (Fig. 5D) clearly exceeds those of BNBI and VU591 (Fig. 5E-F). The VU590 linker is bulkier, more flexible and, therefore, may access additional, less-selective and lower-affinity binding sites in Kir7.1 due to these properties. We postulate that the more rigid imidazole scaffold of BNBI and VU591 contributes to increased selectivity for ROMK inhibition since the demonstrably more flexible VU590 has additional activity at Kir7.1. These issues will be addressed in future studies to define the VU590 and VU591 structure-activity relationships and molecular binding sites in ROMK and Kir7.1.

Downloaded from molpharm.aspetjournals.org at ASPET Journals on April 18, 2024

Molecular Pharmacology Fast Forward. Published on October 6, 2010 as DOI: 10.1124/mol.110.066928
This article has not been copyedited and formatted. The final version may differ from this version.

ACKNOWLEDGEMENTS

We wish to thank Sreedatta Banerjee and members of the Nanion team for expert technical assistance, Dr. Eric Delpire for providing oocytes, Aihua Bian (Vanderbilt University Department of Biostatistics) for assistance with multivariate statistical analysis and members of the Kupershmidt laboratory for advice on hERG recordings.

Downloaded from molpharm.aspetjournals.org at ASPET Journals on April 18, 2024

Molecular Pharmacology Fast Forward. Published on October 6, 2010 as DOI: 10.1124/mol.110.066928
This article has not been copyedited and formatted. The final version may differ from this version.

AUTHOR CONTRIBUTIONS

G.B., B.A.C., W.L., E.S.D., R.K., L.M.L., J.M., C.D.W., L.M.S., C.W.L., J.S.D. designed research; G.B., B.A.C., W.L., E.S.D., R.K., L.M.L. performed research, B.A.C., E.S.D., J.M. contributed new reagents or analytical tools; G.B., B.A.C., W.L., E.S.D., R.K., L.M.L, L.M.S., J.S.D. analyzed data; B.A.C., E.S.D., L.M.S., J.S.D. wrote the paper.

Downloaded from molpharm.aspetjournals.org at ASPET Journals on April 18, 2024

Molecular Pharmacology Fast Forward. Published on October 6, 2010 as DOI: 10.1124/mol.110.066928
This article has not been copyedited and formatted. The final version may differ from this version.

REFERENCES

Bartter FC, Pronove P, Gill JR, Jr. and Maccardle RC (1962) Hyperplasia of the juxtaglomerular complex with hyperaldosteronism and hypokalemic alkalosis. A new syndrome. *Am J Med* **33**:811-828.

Bhave G, Lonergan, D., Chauder, B.A. and Denton, JS (2010) Small-molecule modulators of inward rectifying potassium channels: recent progress and future possibilities. *Future Medicinal Chemistry* **2**(5):757-774.

Carrisoza-Gaytan R, Salvador C, Satlin LM, Liu W, Zavilowitz B, Bobadilla NA, Trujillo J and Escobar LI Potassium secretion by voltage-gated potassium channel Kv1.3 in the rat kidney. *Am J Physiol Renal Physiol* **299**(1):F255-264.

Chuang HH, Jan YN and Jan LY (1997) Regulation of IRK3 inward rectifier K^+ channel by m1 acetylcholine receptor and intracellular magnesium. *Cell* **89**(7):1121-1132.

Clark MA, Humphrey SJ, Smith MP and Ludens JH (1993) Unique natriuretic properties of the ATP-sensitive K^+-channel blocker glyburide in conscious rats. *J Pharmacol Exp Ther* **265**(2):933-937.

Fallen K, Banerjee S, Sheehan J, Addison D, Lewis LM, Meiler J and Denton JS (2009) The Kir channel immunoglobulin domain is essential for Kir1.1 (ROMK) thermodynamic stability, trafficking and gating. *Channels (Austin)* **3**(1):57-68.

Grimm PR and Sansom SC (2007) BK channels in the kidney. *Curr Opin Nephrol Hypertens* **16**(5):430-436.

Grobbee DE and Hoes AW (1995) Non-potassium-sparing diuretics and risk of sudden cardiac death. *J Hypertens* **13**(12 Pt 2):1539-1545.

Hebert SC, Desir G, Giebisch G and Wang W (2005) Molecular diversity and regulation of renal potassium channels. *Physiol Rev* **85**(1):319-371.

Downloaded from molpharm.aspetjournals.org at ASPET Journals on April 18, 2024

Molecular Pharmacology Fast Forward. Published on October 6, 2010 as DOI: 10.1124/mol.110.066928
This article has not been copyedited and formatted. The final version may differ from this version.

Ho K, Nichols CG, Lederer WJ, Lytton J, Vassilev PM, Kanazirska MV and Hebert SC (1993) Cloning and expression of an inwardly rectifying ATP-regulated potassium channel. *Nature* **362**(6415):31-38.

Jain AN (2000) Morphological similarity: a 3D molecular similarity method correlated with protein-ligand recognition. *J Comput Aided Mol Des* **14**(2):199-213.

Ji W, Foo JN, O'Roak BJ, Zhao H, Larson MG, Simon DB, Newton-Cheh C, State MW, Levy D and Lifton RP (2008) Rare independent mutations in renal salt handling genes contribute to blood pressure variation. *Nat Genet* **40**(5):592-599.

Jiang B, Sun X, Cao K and Wang R (2002) Endogenous Kv channels in human embryonic kidney (HEK-293) cells. *Mol Cell Biochem* **238**(1-2):69-79.

Lewis LM, Bhave G, Chauder BA, Banerjee S, Lornsen KA, Redha R, Fallen K, Lindsley CW, Weaver CD and Denton JS (2009) High-throughput screening reveals a small-molecule inhibitor of the renal outer medullary potassium channel and Kir7.1. *Mol Pharmacol* **76**(5):1094-1103.

Lu M, Wang T, Yan Q, Wang W, Giebisch G and Hebert SC (2004) ROMK is required for expression of the 70-pS K channel in the thick ascending limb. *Am J Physiol Renal Physiol* **286**(3):F490-495.

Macdonald JE and Struthers AD (2004) What is the optimal serum potassium level in cardiovascular patients? *J Am Coll Cardiol* **43**(2):155-161.

Milligan CJ, Li J, Sukumar P, Majeed Y, Dallas ML, English A, Emery P, Porter KE, Smith AM, McFadzean I, Beccano-Kelly D, Bahnasi Y, Cheong A, Naylor J, Zeng F, Liu X, Gamper N, Jiang LH, Pearson HA, Peers C, Robertson B and Beech DJ (2009) Robotic multiwell planar patch-clamp for native and primary mammalian cells. *Nat Protoc* **4**(2):244-255.

Downloaded from molpharm.aspetjournals.org at ASPET Journals on April 18, 2024

Molecular Pharmacology Fast Forward. Published on October 6, 2010 as DOI: 10.1124/mol.110.066928
This article has not been copyedited and formatted. The final version may differ from this version.

Ookata K, Tojo A, Suzuki Y, Nakamura N, Kimura K, Wilcox CS and Hirose S (2000) Localization of inward rectifier potassium channel Kir7.1 in the basolateral membrane of distal nephron and collecting duct. *J Am Soc Nephrol* **11**(11):1987-1994.

Peters M, Jeck N, Reinalter S, Leonhardt A, Tonshoff B, Klaus GG, Konrad M and Seyberth HW (2002) Clinical presentation of genetically defined patients with hypokalemic salt-losing tubulopathies. *Am J Med* **112**(3):183-190.

Pluznick JL, Wei P, Carmines PK and Sansom SC (2003) Renal fluid and electrolyte handling in BKCa-beta1$^{-/-}$ mice. *Am J Physiol Renal Physiol* **284**(6):F1274-1279.

Rieg T, Vallon V, Sausbier M, Sausbier U, Kaissling B, Ruth P and Osswald H (2007) The role of the BK channel in potassium homeostasis and flow-induced renal potassium excretion. *Kidney Int* **72**(5):566-573.

Simon DB, Karet FE, Rodriguez-Soriano J, Hamdan JH, DiPietro A, Trachtman H, Sanjad SA and Lifton RP (1996) Genetic heterogeneity of Bartter's syndrome revealed by mutations in the K^+ channel, ROMK. *Nat Genet* **14**(2):152-156.

Tobin MD, Tomaszewski M, Braund PS, Hajat C, Raleigh SM, Palmer TM, Caulfield M, Burton PR and Samani NJ (2008) Common variants in genes underlying monogenic hypertension and hypotension and blood pressure in the general population. *Hypertension* **51**(6):1658-1664.

Wang L, Feng ZP, Kondo CS, Sheldon RS and Duff HJ (1996) Developmental changes in the delayed rectifier K^+ channels in mouse heart. *Circ Res* **79**(1):79-85.

Wang T, Wang WH, Klein-Robbenhaar G and Giebisch G (1995a) Effects of a novel K_{ATP} channel blocker on renal tubule function and K^+ channel activity. *J Pharmacol Exp Ther* **273**(3):1382-1389.

Downloaded from molpharm.aspetjournals.org at ASPET Journals on April 18, 2024

Molecular Pharmacology Fast Forward. Published on October 6, 2010 as DOI: 10.1124/mol.110.066928
This article has not been copyedited and formatted. The final version may differ from this version.

Wang T, Wang WH, Klein-Robbenhaar G and Giebisch G (1995b) Effects of glyburide on renal tubule transport and potassium-channel activity. *Ren Physiol Biochem* **18**(4):169-182.

Wang W and Lu M (1995) Effect of arachidonic acid on activity of the apical K^+ channel in the thick ascending limb of the rat kidney. *J Gen Physiol* **106**(4):727-743.

Welling PA and Ho K (2009) A comprehensive guide to the ROMK potassium channel: form and function in health and disease. *Am J Physiol Renal Physiol* **297**(4):F849-863.

Witchel HJ, Milnes JT, Mitcheson JS and Hancox JC (2002) Troubleshooting problems with in vitro screening of drugs for QT interval prolongation using HERG K^+ channels expressed in mammalian cell lines and Xenopus oocytes. *J Pharmacol Toxicol Methods* **48**(2):65-80.

Yu SP and Kerchner GA (1998) Endogenous voltage-gated potassium channels in human embryonic kidney (HEK293) cells. *Journal of Neuroscience Research* **52**(5):612-617.

Zhou H, Tate SS and Palmer LG (1994) Primary structure and functional properties of an epithelial K channel. *Am J Physiol* **266**(3 Pt 1):C809-824.

Downloaded from molpharm.aspetjournals.org at ASPET Journals on April 18, 2024

Molecular Pharmacology Fast Forward. Published on October 6, 2010 as DOI: 10.1124/mol.110.066928
This article has not been copyedited and formatted. The final version may differ from this version.

FOOTNOTES:

G.B. and B.A.C. contributed equally. This work was supported by National Institutes of health Grants [1R21NS57041-1, 1R01-DK082884, R01-GM080403, DK038470, U54MH074427, 1U54MH084659, P30DK079307, T32GM07628], an American Heart Association Southeast Affiliate Beginning Grant-in-Aid [0865106E] and a National Kidney Foundation Postdoctoral Fellowhip.

Downloaded from molpharm.aspetjournals.org at ASPET Journals on April 18, 2024

Molecular Pharmacology Fast Forward. Published on October 6, 2010 as DOI: 10.1124/mol.110.066928
This article has not been copyedited and formatted. The final version may differ from this version.

FIGURE LEGENDS

Figure 1. BNBI inhibits ROMK but not Kir7.1. Representative whole-cell patch clamp experiment showing dose-dependent inhibition of ROMK-S44D by bis-nitrobenzimidazole (BNBI). Normalized current ($I_{BNBI}/I_{Control}$) recorded at -120 mV is shown. Barium (Ba; 2 mM) was used to measure leak current at the end of every experiment. Data shown in 1A-B were acquired using a Patchliner automated patch clamp workstation (see Methods). (B) Mean ± SEM concentration-response data for BNBI (n=5) and VU590 (n=5) are shown for comparison. (C) Mean ± SEM percent inhibition by VU590 (10 μM) and BNBI (100 μM) of Kir7.1 current at -120 mV in conventional patch clamp experiments (n=3-4).

Figure 2. Development of a BNBI analog with improved potency toward ROMK. (A) Molecular structures of VU590, BNBI and VU591. Atom connectivity is shown in bold to highlight regions of common topology. (B) Concentration-response curves for BNBI (open circles) and VU591 (closed circles) mediated inhibition of Tl^+ flux through ROMK-S44D. Means ± SEM (n=5). (C) Representative time course of 10 μM VU591-dependent ROMK inhibition, incomplete washout and block by 2 mM barium (Ba). Cells were voltage ramped between -120 mV and 120 mV at a rate of 2.4 mV/msec every 5 sec from a holding potential of -75 mV (inset). Current at -120 mV are shown. (D) ROMK current-voltage relationship recorded in the absence (control) or during steady-state block by 10 μM VU591.

Figure 3. VU591 is a ROMK channel pore blocker. (A) Representative whole cell current responses to voltage steps from a holding potential of -80 mV (see protocol in D)

Downloaded from molpharm.aspetjournals.org at ASPET Journals on April 18, 2024

Molecular Pharmacology Fast Forward. Published on October 6, 2010 as DOI: 10.1124/mol.110.066928
This article has not been copyedited and formatted. The final version may differ from this version.

in a bath solution with [K^+] of 5 mM recorded in rat ROMK transiently transfected HEK293 cells. Left panel is in control conditions, middle panel with 10 μM VU591, and right panel with 1 μM TPNQ. (B) Representative whole cell current traces with voltage steps from a holding potential of -20 mV (see protocol in D) in a bath solution with [K^+] of 50 mM recorded in rat ROMK1 transiently transfected HEK293 cells. Left panel is in control conditions, middle panel with 10 μM VU591, and right panel with 1 μM TPNQ. (C) Percent VU591 inhibition was calculated at each voltage with 5 mM and 50 mM extracellular K^+ after subtracting leak current defined as residual current with 1 μM TPNQ. Inhibition at the holding potential (-80 mV in 5 mM K^+ and -20 mV in 50 mM K^+) was not determined given the low current amplitudes near E_K. (D) Voltage step protocol involving a holding potential near E_K (-80 mV and -20 mV in 5 mM and 50 mM extracellular K^+ respectively) with first step to 20 mV followed by lower steps in 20 mV increments with intervening periods of 200 ms at the holding potential. Step duration was extended to 5 seconds to reach near steady state conditions particularly in the presence of VU591. (E) Model for VU591 and TPNQ block of ROMK currents (see text for further details).

Figure 4. Metabolic stability of VU591 in human or rat liver microsomes. Percent VU591, Verapamil (control) Propranalol (control) remaining after a 15-min incubation are shown. Data are means ± S.D. from 2 replicate experiments.

Figure 5. Addition of negative surface electrostatic potential through an ether linkage increases ROMK inhibitor potency. Two primary screening hits A) VU590 and B) BNBI share the common substructure of flanking nitrophenyl groups linked by

Downloaded from molpharm.aspetjournals.org at ASPET Journals on April 18, 2024

Molecular Pharmacology Fast Forward. Published on October 6, 2010 as DOI: 10.1124/mol.110.066928
This article has not been copyedited and formatted. The final version may differ from this version.

alkyl chains of different length and composition. Visualization of the distribution of electrostatic properties was achieved by displaying atom-centered point charges from the Merck Molecular Mechanics Forcefield (MMFF94) on a Connolly surface of each molecule (Panels A-C). Atomic charge values are indicated by color ramp ranges from negative (red) to positive electrostatic potential (blue). When VU590 is flexibly aligned with BNBI (see Methods) and displayed in a similar conformation, localization of negative electrostatic potential in the middle portion of the molecule is observed. This is consistent with the rationale used to generate increased potency in C) VU591 and suggests that the negative electrostatic potential of the ether linker contributes to the increased potency of VU591 toward ROMK. Right-hand panels illustrate conformational ensembles generated by SurflexSim (SybylX 1.1, Tripos) from the top 10 scoring aligned conformers of D) VU590, E) BNBI and F) VU591. The surface of the best scoring, most similar alignment (grey Connolly surface) highlights Increased flexibility within and flanking the VU590 macrocyclic linker relative to the bicyclic rings and propyl/ether linker of BNBI/VU591 that is consistent with enhanced ROMK selectivity observed experimentally with VU591 versus VU590.

Downloaded from molpharm.aspetjournals.org at ASPET Journals on April 18, 2024

Molecular Pharmacology Fast Forward. Published on October 6, 2010 as DOI: 10.1124/mol.110.066928
This article has not been copyedited and formatted. The final version may differ from this version.

Table 1. VU591 is a selective ROMK channel inhibitor. Mean ± S.E.M. percent inhibition by VU591 of the indicated K^+ channel. Whole-cell currents were recorded from HEK-293 cells transfected with rat (n=4-8) or human (n=4) ROMK1, human Kir2.1 (n=6), human Kir2.3 (n=5), human Kir4.1 (n=4), mouse Kir6.2/hamster SUR1 (n=3-5), human Kir7.1 (n=4), Slo1/β1 (n=4), Kv1.3 (n=4). *hERG currents (n=6) were recorded from *Xenopus* oocytes. Voltage clamp protocols are described in Methods. Barium (2 mM), tetraethylammonium (2 mM), 4-aminopyridine (1 mM) or Dofetilide (10 μM) were used as control blockers of KirX, Slo1/β1, Kv1.3 and hERG, respectively. The mean ± S.E.M. percent inhibition were: rROMK (94 ± 2; n=8); hROMK (96 ± 1; n=4); Kir2.1 (98 ± 1; n=6); Kir4.1 (96 ± 2; n=4); Kir6.2/SUR1B (98 ± 1; n=8); Kir7.1 (91 ± 2; n=4); Slo1/β1 (72 ± 3; n=4); Kv1.3 (73 ± 6; n=4); hERG (94 ± 1; n=8). Representative current traces for KirX, Slo1/β1, Kv1.3 and hERG are shown in suporting Figs. S2-S5, respectively.

Channel	[VU591] μM	% Inhibition (Mean ± S.E.M.)
rROMK	0.3	54 ± 4
rROMK	1	63 ± 2
rROMK	3	77 ± 4
rROMK	10	89 ± 1
rROMK	30	91 ± 2
hROMK	10	86 ± 2
Kir2.1	10	-4 ± 3
Kir2.3	10	6 ± 6
Kir4.1	10	-10 ± 4
Kir6.2/SUR1B	10	17 ± 4
Kir6.2/SUR1B	50	28 ± 3
Kir7.1	10	5 ± 8
Slo1/β1	10	-4 ± 2
Kv1.3	10	-5 ± 4
*hERG	10	25 ± 2

Downloaded from molpharm.aspetjournals.org at ASPET Journals on April 18, 2024

Molecular Pharmacology Fast Forward. Published on October 6, 2010 as DOI: 10.1124/mol.110.066928
This article has not been copyedited and formatted. The final version may differ from this version.

Table 2. Plasma protein binding of VU591. Percent VU591, Warfarin (control) and Verapamil (control) bound to human or rat serum protein are shown. Data are means ± S.D. from 2 replicate experiments.

	Human (% bound)	Rat (% bound)
VU591	99.14 ± 0.0056	98.39 ± 0.0010
Warfarin	99.62 ± 0.0002	99.57 ± 0.0003
Verapamil	93.41 ± 0.0088	97.14 ± 0.0037

Downloaded from molpharm.aspetjournals.org at ASPET Journals on April 18, 2024

Figure 1

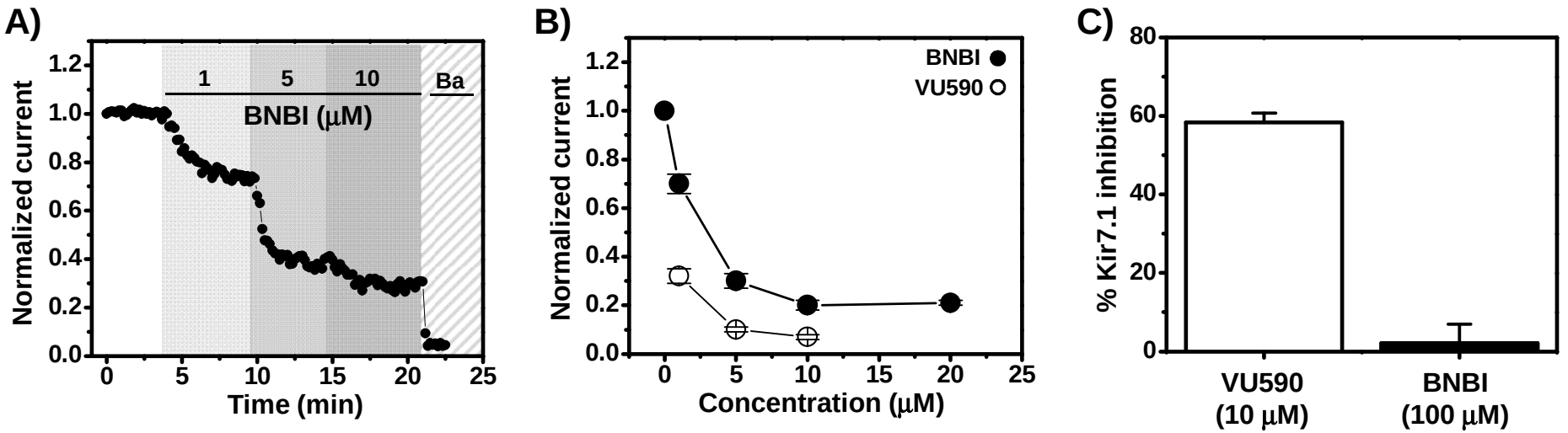

Molecular Pharmacology Fast Forward. Published on October 6, 2010 as DOI: 10.1124/mol.110.066928
This article has not been copyedited and formatted. The final version may differ from this version.

Downloaded from molpharm.aspetjournals.org at ASPET Journals on April 18, 2024

Figure 2

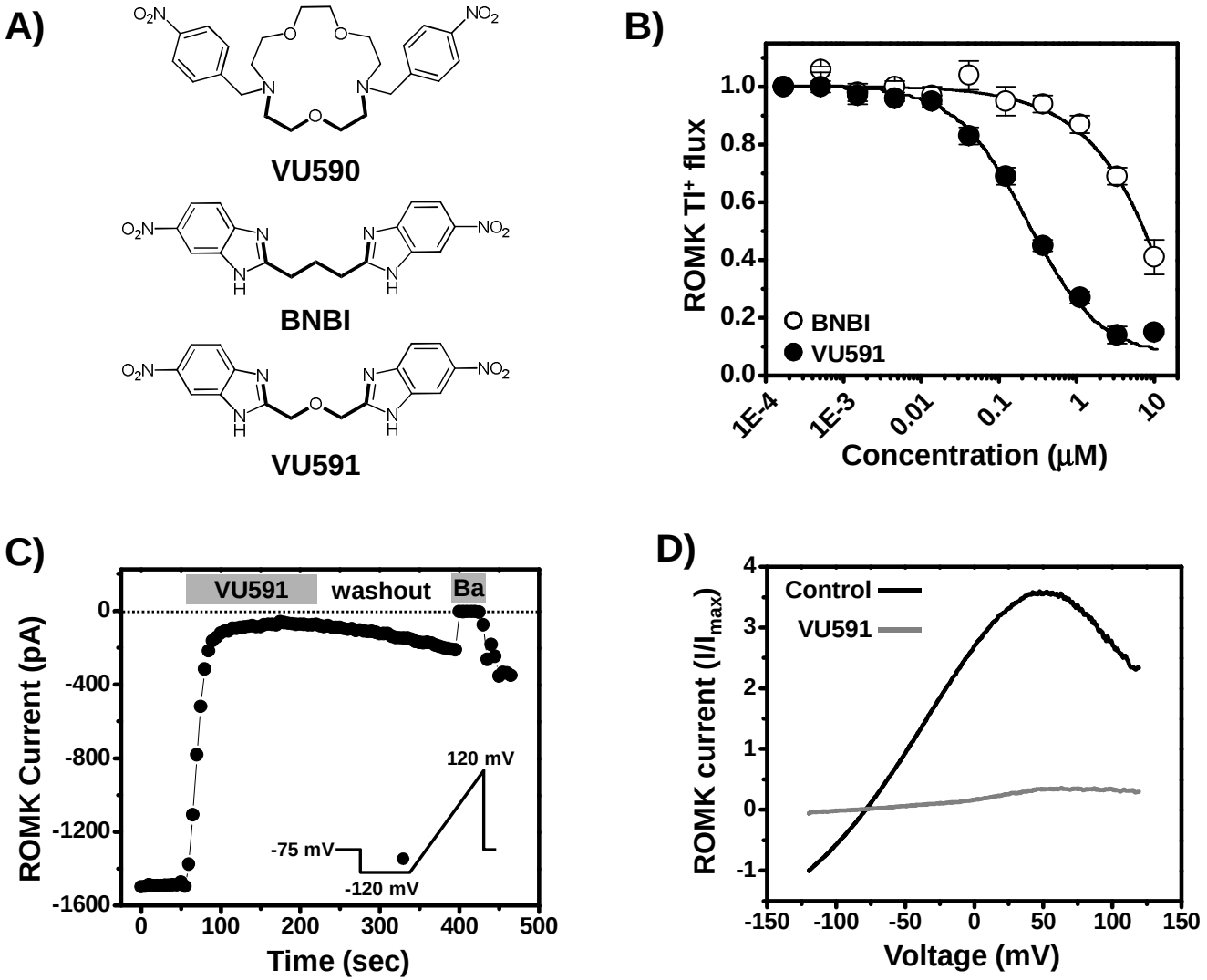

Molecular Pharmacology Fast Forward. Published on October 6, 2010 as DOI: 10.1124/mol.110.066928
This article has not been copyedited and formatted. The final version may differ from this version.

Downloaded from molpharm.aspetjournals.org at ASPET Journals on April 18, 2024

Figure 3

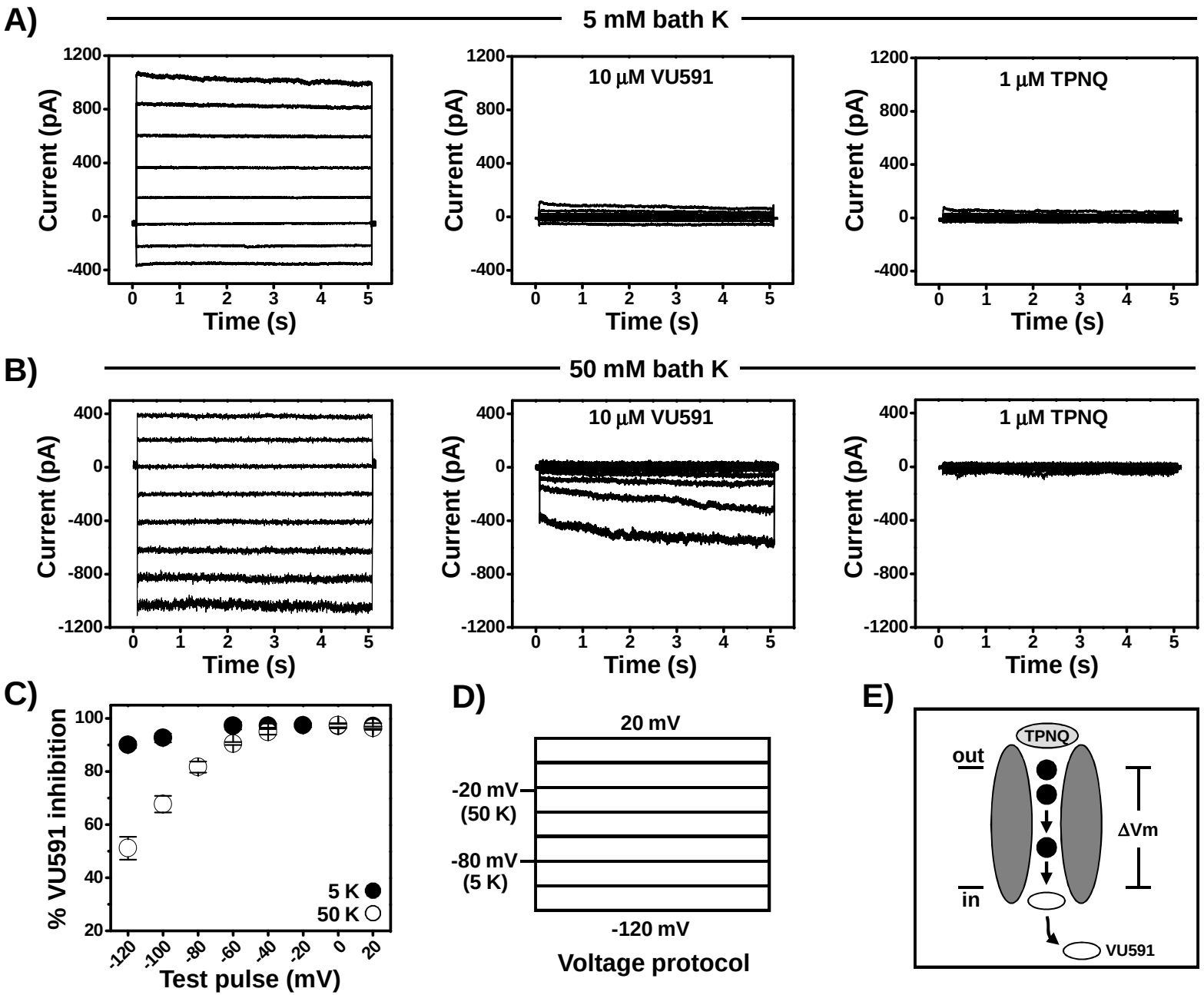

Molecular Pharmacology Fast Forward. Published on October 6, 2010 as DOI: 10.1124/mol.110.066928
This article has not been copyedited and formatted. The final version may differ from this version.

Downloaded from molpharm.aspetjournals.org at ASPET Journals on April 18, 2024

Figure 4

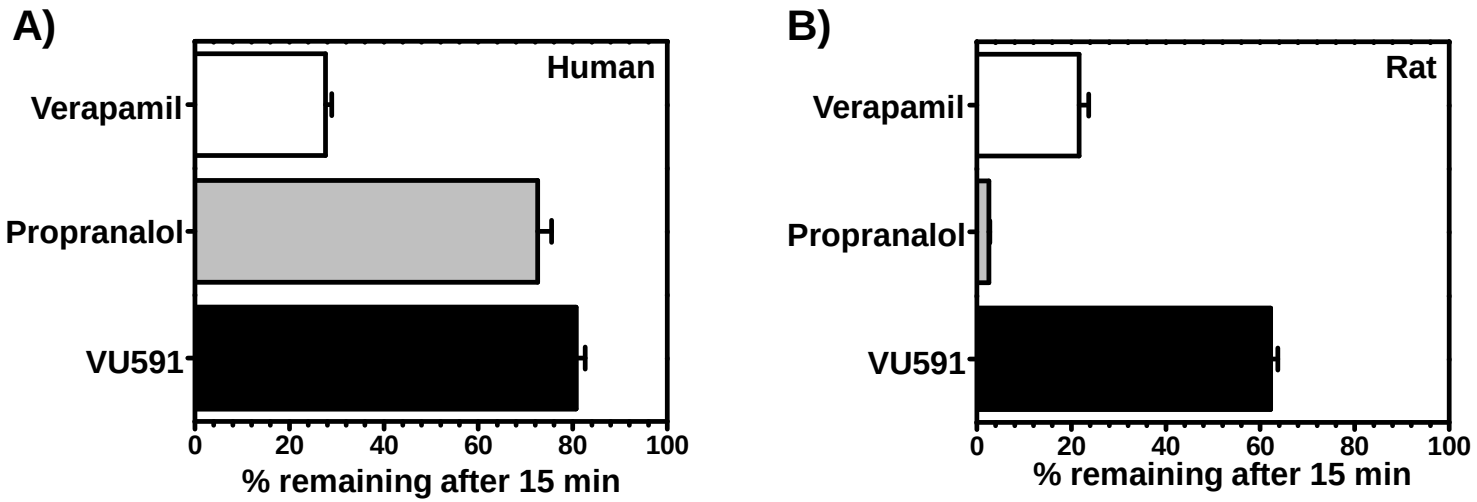

Molecular Pharmacology Fast Forward. Published on October 6, 2010 as DOI: 10.1124/mol.110.066928
This article has not been copyedited and formatted. The final version may differ from this version.

Downloaded from molpharm.aspetjournals.org at ASPET Journals on April 18, 2024

Figure 5

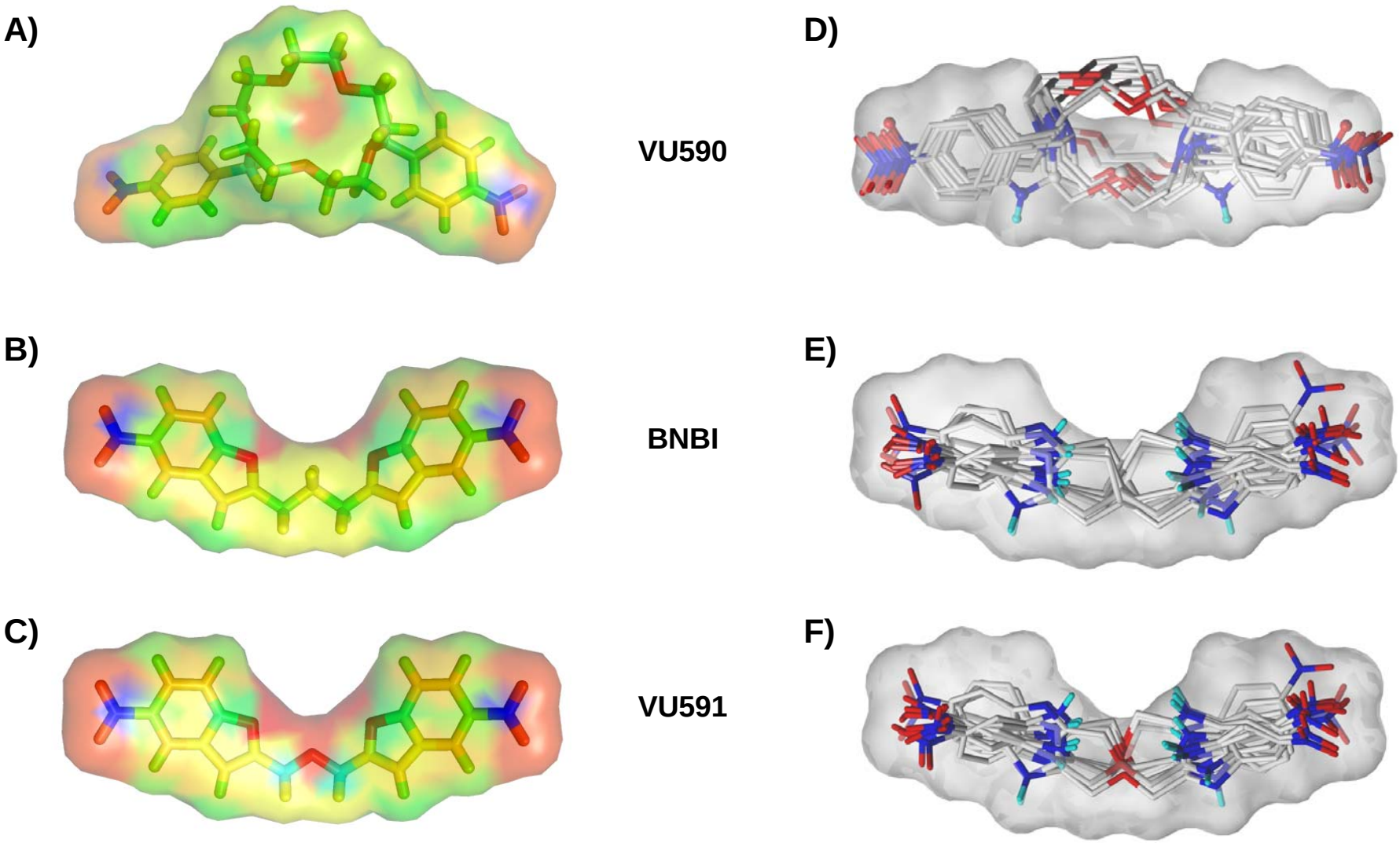

Molecular Pharmacology Fast Forward. Published on October 6, 2010 as DOI: 10.1124/mol.110.066928
This article has not been copyedited and formatted. The final version may differ from this version.

Downloaded from molpharm.aspetjournals.org at ASPET Journals on April 18, 2024

Development of a selective small-molecule inhibitor of Kir1.1, the Renal Outer Medullary Potassium Channel. Gautam Bhave, Brian A. Chauder, Wen Liu, Eric S. Dawson, Rishin Kadakia, Thuy, T. Nguyen, L. Michelle Lewis, Jens Meiler, C. David Weaver, Lisa M. Satlin, Craig W. Lindsley, and Jerod S. Denton. *Molecular Pharmacology.*

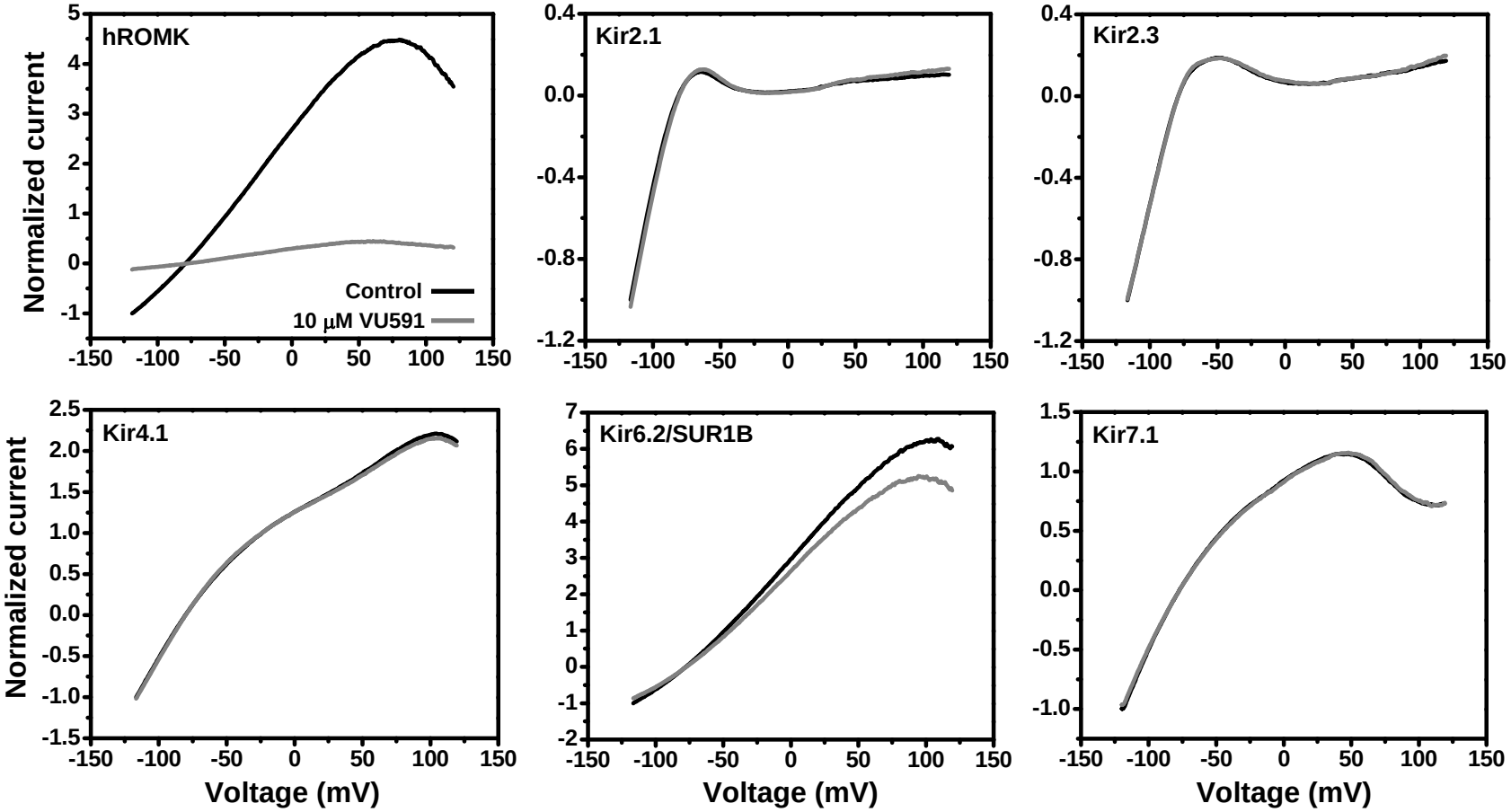

Supplemental Figure 1. Current traces evoked from HEK-293 cells expressing the Kir channel indicated. Cells were voltage ramped between -120 mV and 120 mV at a rate of 2.4 mV/msec every 5 sec from a holding potential of -75 mV. Representative current traces recorded in the absence (control) or presence of 10 μM VU591 are shown.

Development of a selective small-molecule inhibitor of Kir1.1, the Renal Outer Medullary Potassium Channel. Gautam Bhave, Brian A. Chauder, Wen Liu, Eric S. Dawson, Rishin Kadakia, Thuy, T. Nguyen, L. Michelle Lewis, Jens Meiler, C. David Weaver, Lisa M. Satlin, Craig W. Lindsley, and Jerod S. Denton. *Molecular Pharmacology.*

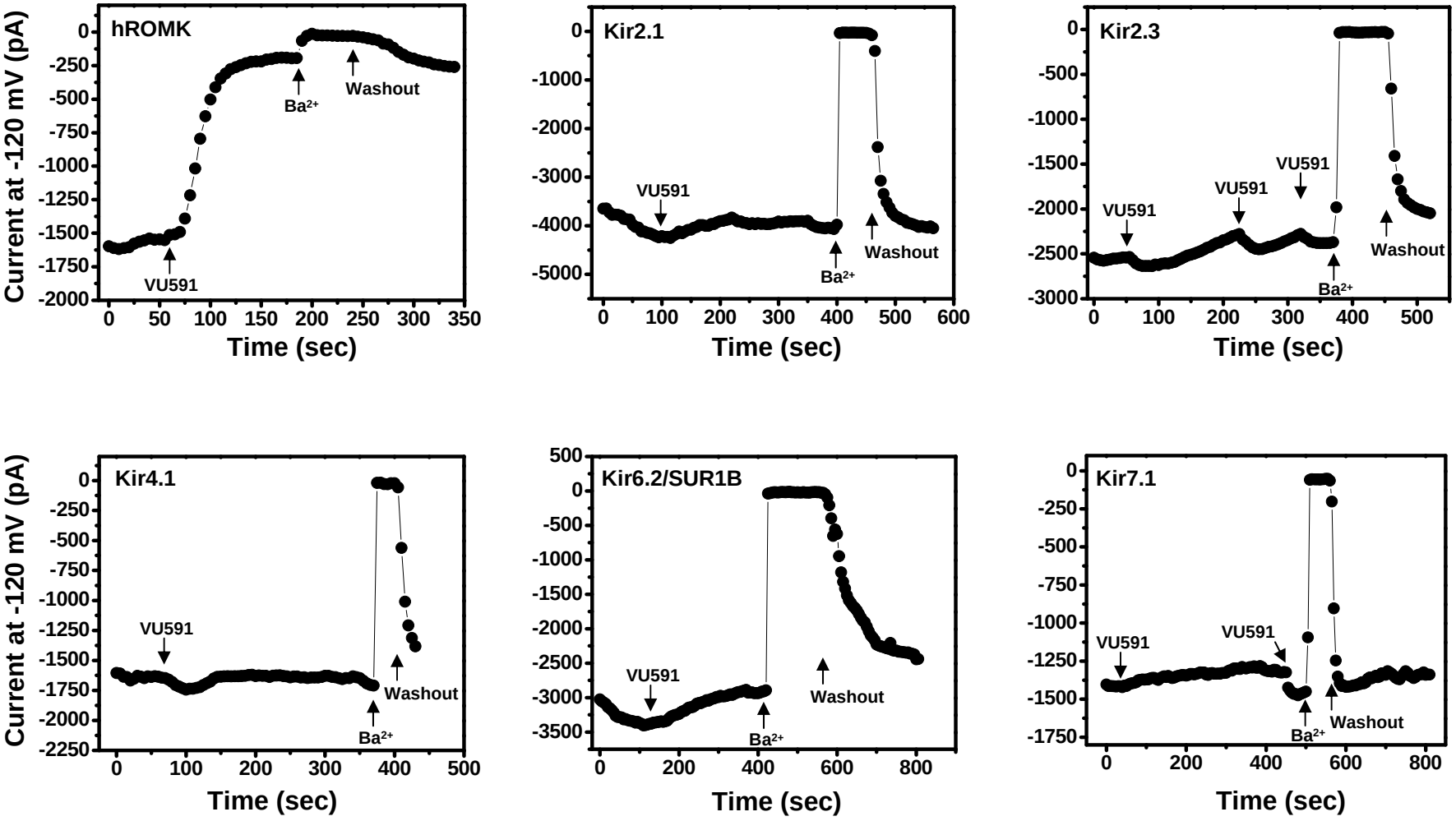

Supplemental Figure 2. Representative time course data showing the effects of 10 μM VU591 or 2 mM barium (Ba^{2+}; control blocker) on the indicated Kir channel expressed in HEK-293 cells. The cells were voltage clamped using the protocol described in supporting Fig. S1 legend. Current recorded at -120 mV is shown.

Development of a selective small-molecule inhibitor of Kir1.1, the Renal Outer Medullary Potassium Channel. Gautam Bhave, Brian A. Chauder, Wen Liu, Eric S. Dawson, Rishin Kadakia, Thuy, T. Nguyen, L. Michelle Lewis, Jens Meiler, C. David Weaver, Lisa M. Satlin, Craig W. Lindsley, and Jerod S. Denton. *Molecular Pharmacology.*

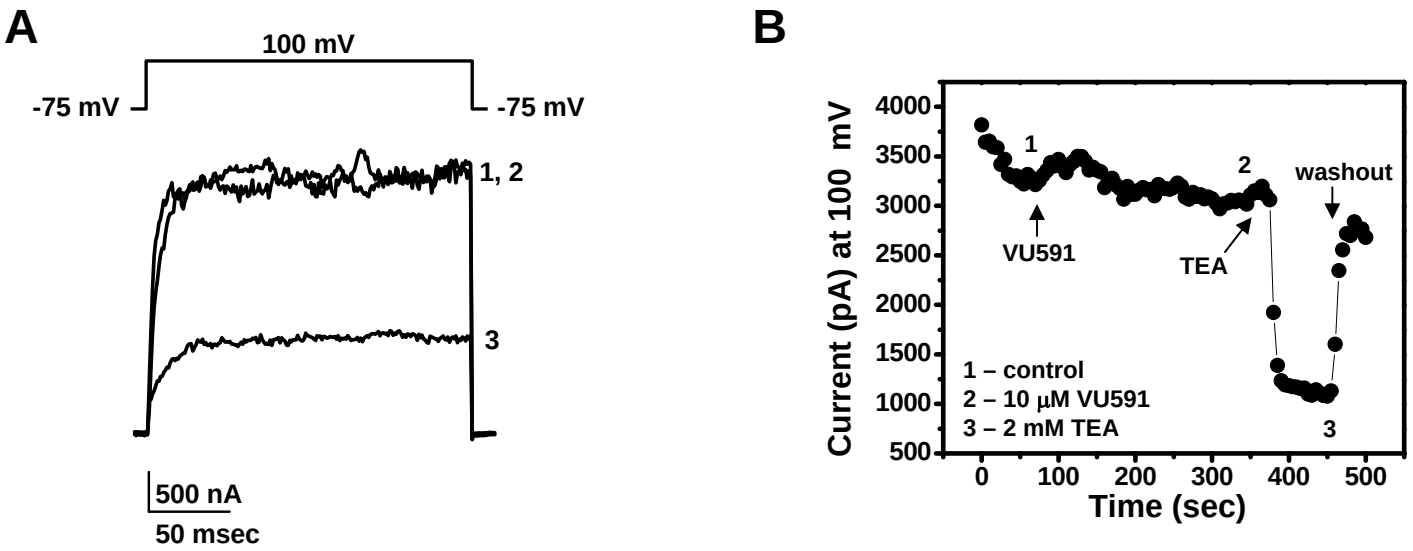

Supplemental Figure 3. (A) Representative BK Slo1/b1 current traces evoked from HEK-293 cells using the voltage clamp protocol shown. Current traces 1 (control), 2 (10 μM VU591) and 3 (2 mM TEA) were taken from the time course experiment shown in (B) where indicated with the corresponding numbers.

Development of a selective small-molecule inhibitor of Kir1.1, the Renal Outer Medullary Potassium Channel. Gautam Bhave, Brian A. Chauder, Wen Liu, Eric S. Dawson, Rishin Kadakia, Thuy, T. Nguyen, L. Michelle Lewis, Jens Meiler, C. David Weaver, Lisa M. Satlin, Craig W. Lindsley, and Jerod S. Denton. *Molecular Pharmacology.*

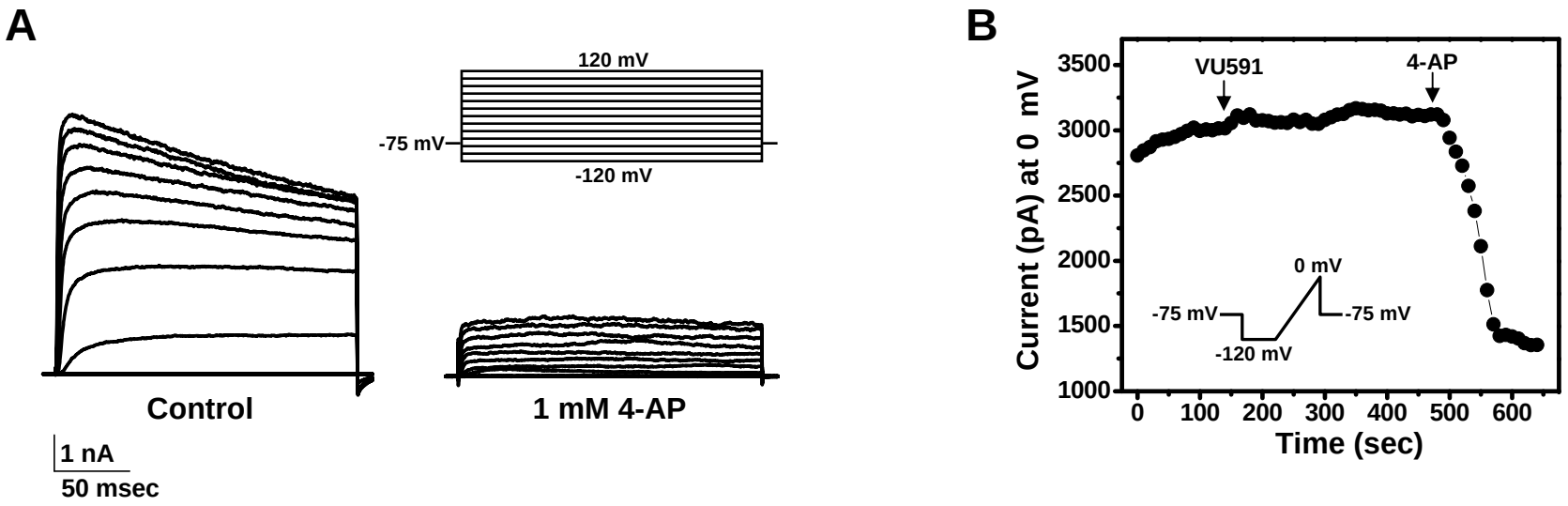

Supplemental Figure 4. (A) Whole-cell Kv1.3 current traces recorded in the absence (control) or presence of 1 mM 4-AP. Currents were evoked using the voltage clamp protocol shown. (B) Representative time course data showing no effect of 10 μM VU591 on Kv1.3 current at 100 mV.

Development of a selective small-molecule inhibitor of Kir1.1, the Renal Outer Medullary Potassium Channel. Gautam Bhave, Brian A. Chauder, Wen Liu, Eric S. Dawson, Rishin Kadakia, Thuy, T. Nguyen, L. Michelle Lewis, Jens Meiler, C. David Weaver, Lisa M. Satlin, Craig W. Lindsley, and Jerod S. Denton. *Molecular Pharmacology.*

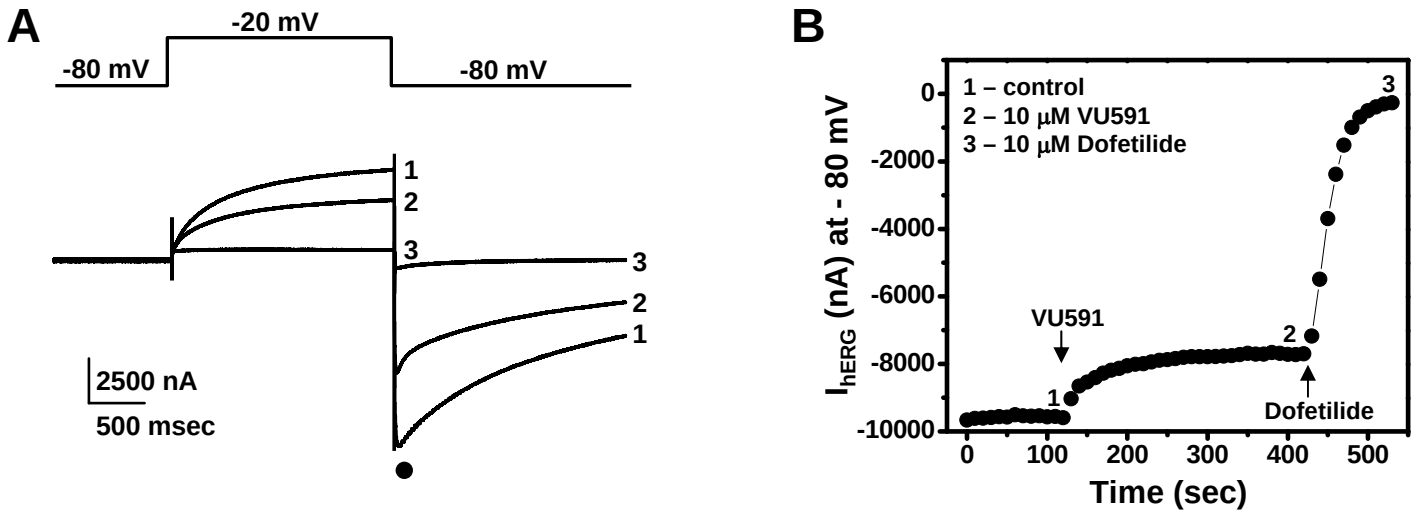

Supplemental Figure 5. (A) Whole-cell hERG current traces evoked from *Xenopus* oocytes using the voltage clamp protocol shown. Current traces 1 (control), 2 (10 μM VU591) and 3 (10 μM Dofetilide) were taken from the time course experiment shown in (B) where indicated with the corresponding numbers. Tail current at -80 mV is shown.

Development of a selective small-molecule inhibitor of Kir1.1, the Renal Outer Medullary Potassium Channel. Gautam Bhave, Brian A. Chauder, Wen Liu, Eric S. Dawson, Rishin Kadakia, Thuy, T. Nguyen, L. Michelle Lewis, Jens Meiler, C. David Weaver, Lisa M. Satlin, Craig W. Lindsley, and Jerod S. Denton. *Molecular Pharmacology.*

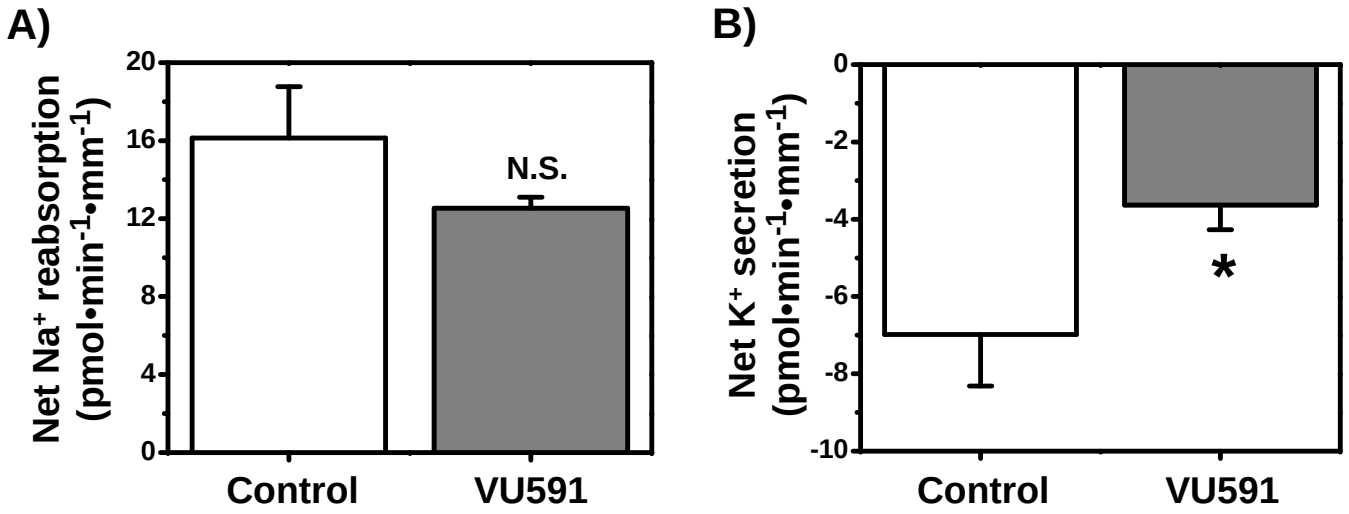

Supplemental Figure 6. Effect of VU591 on cation transport in microperfused rat CCDs. Net Na^+ (A) and K^+ (B) transport were measured in the absence (control) or presence of 10 μM VU591 at constant flow rate of 1 $nl \cdot min^{-1} \cdot mm^{-1}$. Means ± SEM. *P<0.05 vs. transport rate in control conditions from the same CCDs. N.S. Not statistically significant (P>0.05). (n=4).

Development of a selective small-molecule inhibitor of Kir1.1, the Renal Outer Medullary Potassium Channel. Gautam Bhave, Brian A. Chauder, Wen Liu, Eric S. Dawson, Rishin Kadakia, Thuy, T. Nguyen, L. Michelle Lewis, Jens Meiler, C. David Weaver, Lisa M. Satlin, Craig W. Lindsley, and Jerod S. Denton. *Molecular Pharmacology.*

SUPPLEMENTAL METHODS

Animals. Pathogen-free Sprague-Dawley (SD) rats of either sex (~3 wk old; Taconic Farms, Inc., Germantown, NY) were housed in the animal care facility at the Mount Sinai School of Medicine (Center for Comparative Medicine). All animals were allowed free access to tap water and standard rat chow. Animals were euthanized in accordance with the National Institutes of Health Guidelines for the Care and Use of Laboratory Animals. Animal protocols were approved by the IACUC Committee at the Mount Sinai School of Medicine as appropriate.

Microperfusion of Isolated Rat Cortical Collecting Ducts. Kidneys were removed via a midline incision, and single tubules dissected freehand in cold (4^oC) Ringer's solution containing (in mM): 135 NaCl, 2.5 K_2HPO_4, 2.0 $CaCl_2$, 1.2 $MgSO_4$, 4.0 lactate, 6.0 L-alanine, 5.0 HEPES, and 5.5 D-glucose, pH 7.4, 290±2 mOsm/kg, as previously described (Liu et al., 2003). A single tubule was studied from each animal. Isolated collecting ducts (CD) were microperfused *in vitro* as previously described (Liu et al., 2003; Woda et al., 2003). Briefly, each isolated tubule was immediately transferred to a temperature and O_2/CO_2-controlled specimen chamber, mounted on concentric glass pipettes, and perfused and bathed at 37^oC with Burg's perfusate containing (in mM): 120 NaCl, 25 $NaHCO_3$, 2.5 K_2HPO_4, 2.0 $CaCl_2$, 1.2 $MgSO_4$, 4.0 Na lactate, 1.0 Na_3 citrate, 6.0 L-alanine, and 5.5 D-glucose, pH 7.4, 290 ± 2 mOsm/kg (Liu et al., 2003). During

the 30 min equilibration period and thereafter, the perfusion chamber was continuously suffused with a gas mixture of 95% O_2-5% CO_2 to maintain pH of the Burg's solution at 7.4 at 37^{o}C. The bathing solution was exchanged continuously at a rate of 10 ml/hr using a syringe pump (Razel, Stamford, CT).

Transport measurements were performed in the absence of transepithelial osmotic gradients and thus water transport was assumed to be zero. Three to four samples of tubular fluid were collected under water-saturated light mineral oil by timed filling of a calibrated 15 nl volumetric constriction pipette at each perfusion rate. To determine the concentrations of K^+ and Na^+ delivered to the tubular lumen, ouabain (500 μM) was added to the bath at the conclusion of each experiment to inhibit active transport, and an additional three to four samples of tubular fluid were obtained for analysis. The cation concentrations of perfusate and collected tubular fluid were determined by helium glow photometry and the rates of net transport (Jx, in pmol·min^{-1}·mm^{-1} tubular length) were calculated using standard flux equations, as previously described (Estilo et al., 2008). The calculated ion fluxes were averaged to obtain a single mean rate of ion transport for the CCD under each condition.

Measurements of net cation transport in each CD were performed in the absence and then presence of 10 μM VU591 added to the luminal perfusate. The inhibitor was present for at least 10 min before tubular fluid samples were obtained for experimental measurements. Subsequent samples of tubular fluid were collected in the continuous presence of the inhibitor.

REFERENCES

Estilo G, Liu W, Pastor-Soler N, Mitchell P, Carattino MD, Kleyman TR and Satlin LM (2008) Effect of aldosterone on BK channel expression in mammalian cortical collecting duct. *Am J Physiol Renal Physiol* **295**(3):F780-788.

Liu W, Xu S, Woda C, Kim P, Weinbaum S and Satlin LM (2003) Effect of flow and stretch on the $[Ca^{2+}]_i$ response of principal and intercalated cells in cortical collecting duct. *Am J Physiol Renal Physiol* **285**(5):F998-F1012.

Woda CB, Miyawaki N, Ramalakshmi S, Ramkumar M, Rojas R, Zavilowitz B, Kleyman TR and Satlin LM (2003) Ontogeny of flow-stimulated potassium secretion in rabbit cortical collecting duct: functional and molecular aspects. *Am J Physiol Renal Physiol* **285**(4):F629-639.

Development of a selective small-molecule inhibitor of Kir1.1, the Renal Outer Medullary Potassium Channel. Gautam Bhave, Brian A. Chauder, Wen Liu, Eric S. Dawson, Rishin Kadakia, Thuy, T. Nguyen, L. Michelle Lewis, Jens Meiler, C. David Weaver, Lisa M. Satlin, Craig W. Lindsley, and Jerod S. Denton. *Molecular Pharmacology*.

Receptor/Target	% Displacement
Adenosine A_1	14
Adenosine A_{2A}	13
Adenosine A_3	21
Adrenergic α_{1A}	6
Adrenergic α_{1B}	5
Adrenergic α_{1D}	10
Adrenergic α_{2A}	14
Adrenergic β_1	6
Adrenergic β_2	9
Androgen	10
Bradykinin B_1	14
Bradykinin B_2	-16
Calcium Channel L-Type, Benzothiazepine	22
Calcium Channel L-Type, Dihydropyridine	26
Calcium Channel N-Type	0
Dopamine D_1	-2
Dopamine D_{2S}	-6
Dopamine D_3	1
Dopamine $D_{4.2}$	75
Endothelin ET_A	0
Endothelin ET_B	2
Epidermal Growth Factor (EGF)	5
Estrogen ERα	1
G protein-coupled Receptor GPR103	15
$GABA_A$, Flunitrazepam, Central	77
$GABA_A$, Muscimol, Central	-3
$GABA_{B1A}$	0
Glucocorticoid	3
Glutamate, Kainate	2
Glutamate, NMDA, Agonism	5
Glutamate, NMDA, Glycine	5
Glutamate, NMDA, Phencyclidine	0
Histamine H_1	13
Histamine H_2	0
Histamine H_3	-12
Imidazoline I2, Central	0
Interleukin IL-1	0
Leukotriene, Cysteinyl $CysLT_1$	0
Melatonin MT_1	2
Muscarinic M_1	4

Development of a selective small-molecule inhibitor of Kir1.1, the Renal Outer Medullary Potassium Channel. Gautam Bhave, Brian A. Chauder, Wen Liu, Eric S. Dawson, Rishin Kadakia, Thuy, T. Nguyen, L. Michelle Lewis, Jens Meiler, C. David Weaver, Lisa M. Satlin, Craig W. Lindsley, and Jerod S. Denton. *Molecular Pharmacology*.

Target/Receptor	% Displacement
Muscarinic M_2	-4
Muscarinic M_3	5
Neuropeptide Y Y_1	-1
Neuropeptide Y Y_2	-3
Nicotinic Acetylcholine	13
Nicotinic Acetylcholine α1, Bungarotoxin	-13
Opiate δ (OP1, DOP)	18
Opiate κ (OP2, KOP)	15
Opiate μ (OP3, MOP)	-6
Phorbol Ester	5
Platelet Activating Factor (PAF)	-6
Potassium Channel (Pancreatic K_{ATP})	43
Potassium Channel (hERG)	-3
Prostanoid EP_4	10
Purinergic P_{2X}	-2
Purinergic P_{2Y}	14
Rolipram	9
Serotonin (5-hydroxytryptamine) 5-HT_{1A}	21
Serotonin (5-hydroxytryptamine) 5-HT_3	18
Sigma σ1	28
Sigma σ2	-2
Sodium Channel, Site 2	4
Tachykinin NK_1	5
Thyroid Hormone	6
Transporter, Dopamine (DAT)	59
Transporter, GABA	16
Transporter, Norepinephrine (NET)	56
Serotonin Transporter	1

Supplemental Table 1. Ancillary pharmacology of VU591 versus 68 GPCRs, ion channels and transporters at Ricerca Biosciences Lead Profile Screen.